



MDOT RC-1629

**Remote Monitoring of Fatigue-sensitive
Details on Bridges
(Part II)**

MARCH 2015



Department of Civil & Construction Engineering
College of Engineering and Applied Sciences
Western Michigan University

RESEARCH

Remote Monitoring of Fatigue-sensitive Details on Bridges

Project Manager: Steve Kahl, P.E.

Submitted to:



Submitted by

Upul Attanayake, Ph.D., P.E.
Associate Professor
Western Michigan University
(269) 276 – 3217
upul.attanayake@wmich.edu

Haluk Aktan, Ph.D., P.E.
Professor
Western Michigan University
(269) 276 – 3206
haluk.aktan@wmich.edu

Robert Hay, Ph.D.
TISEC Inc.
Morin Heights, QC, Canada
(450) 226 - 6804
bohay@structuralinsights.com

Necati Catbas, Ph.D., P.E.
Transtek International Group LLC
fncatbas@gmail.com
(321) 945-1786



Western Michigan University
Department of Civil & Construction Engineering
College of Engineering and Applied Sciences
Kalamazoo, MI 49008-5316
Fax: (269) 276 – 3211

5 DATA ANALYSIS AND SYSTEM PERFORMANCE

This chapter presents (a) a set of acoustic emission (AE) data recorded by the monitoring system and data analysis using ICEPAK™, a pattern classifier for use in real-time structural health and reliability monitoring, (b) calculation of effective stress at a web gap detail using weigh-in-motion (WIM) data and refined finite element analysis, (c) calculation of effective stress at a web gap detail using strain data from field monitoring, (d) findings related to monitoring system performance, and (d) a summary.

5.1 ACOUSTIC EMISSION DATA ANALYSIS

The goal was to examine the types of AE signals detected from fatigue-sensitive details to determine, among the different AE signals generated during normal traffic conditions, how to use these signals to assess the performance of the bridge detail.

5.1.1 Data Acquisition

AE data was recorded using four sensors arranged as shown in Figure 4-3 and Figure 4-4. Two sample data files that were recorded on July 09, 2014 and on July 11, 2014, respectively, were used in the data analysis presented in this section. The data represent AE signals captured on the bridge near the fatigue-sensitive detail under normal traffic conditions. PLB signals near the sensors were also recorded for reference.

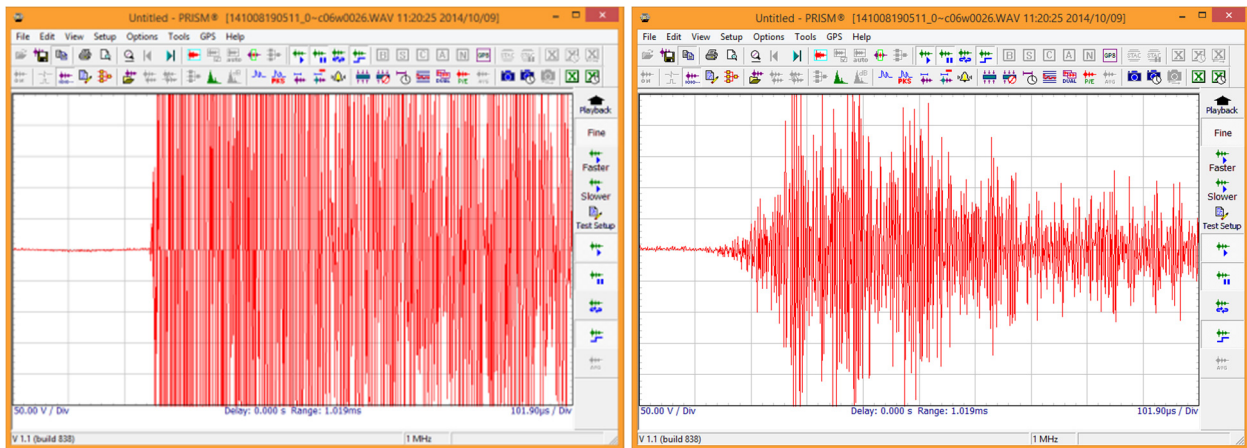
5.1.2 Data Preprocessing

Data generated in the *AE Win* closed proprietary format (“*.dta*”) are not compatible with the ICEPAK™ software developed by TISEC Inc. The TISEC SABRE™ system components include a waveform extraction utility (WEU v 2.1) to convert *AE win* data in a format compatible with ICEPAK™. WEU v 2.1 was also used to convert to a second universal format (*.wav*) that is compatible with the waveform visualization software. The PRISM module enabled waveform visualization in both time and power spectral domains. ICEPAK™ was used to classify data via pre-trained classifiers designed by the ICEPAK software package.

5.1.3 Pencil Lead Break (PLB) Signals

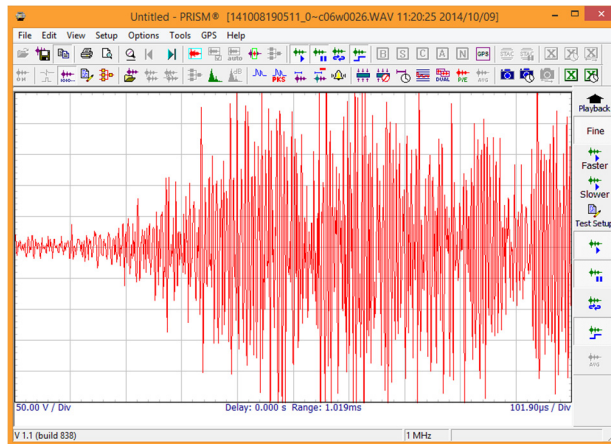
The fracture-event representation signals generated by PLB serve as a reference to identify the presence of any significant fracture type signals within the ensemble of AE data collected under normal traffic conditions.

Typical signals present in a PLB data file are shown in Figure 5-1. The PRISM package can be used for visual inspection after converting the data to PRISM compatible .wav files. Visual inspection of signals is very important to identify the signals that are not suitable for further analysis. One such example is the presence of oversaturated signals. Use of such signals in analysis is known to produce skewed spectral characteristics that prevent reliable signal analysis.



(a) An oversaturated signal

(b) A good signal



(c) A possible noise

Note: X-axis: Time (101.9 µs/Div); Y-axis: Voltage (50 V/Div)

Figure 5-1. Typical signals present in a data file

5.1.4 Unsupervised Learning via Clustering

The data collected from the bridge was examined directly to identify any significant similar AE activity formations using non-linear mapping (NLM) and clustering analysis available in ICEPAK™. NLM presents multi-dimensional data in a 2-D space and preserves the inter-data distance and directional information. If the data in the multi-dimensional space are very close to one another, the corresponding NLM should also render their closeness to one another but not their orientation.

NLM can be performed in time, power, phase, cepstral, and auto-correlation domains. The data set used for NLM and clustering analysis included little more than 11,000 AE signals that were above the set threshold of 45dB. NLM was performed using one feature domain at a time to visually detect significant naturally forming concentrations. These results are shown in Figure 5-2 to Figure 5-6. Out of the 5 domains, the spectral power domain produced three significant concentrations as shown in Figure 5-3. Clustering was performed using the same spectral power domain features, and produced three significant concentrations as presented in Figure 5-7. The clusters are aligned with the visual presentation of the NLM result. In order to make the side-by-side comparison easier, spectral power domain results from NLM and clustering are presented in Figure 5-8 and Figure 5-9. Later, as shown in Figure 5-10, the three clusters that were identified through the power domain analysis were separated for further analysis.

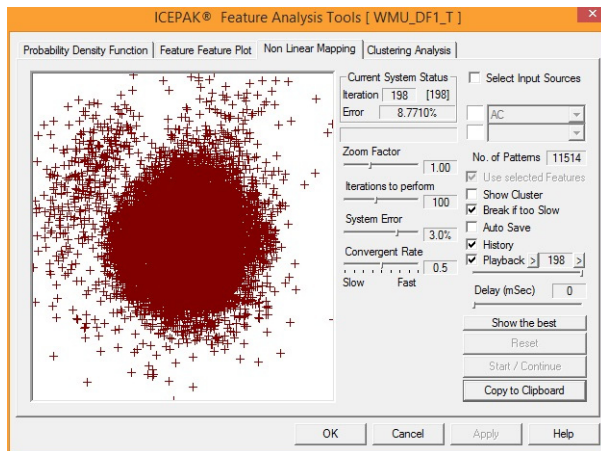


Figure 5-2. NLM Time Domain

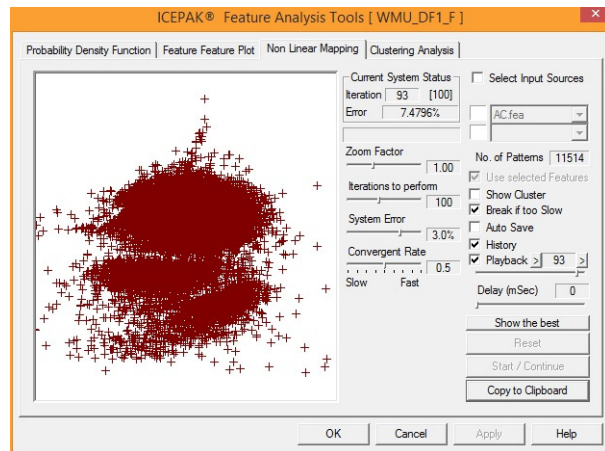


Figure 5-3. NLM Power Domain

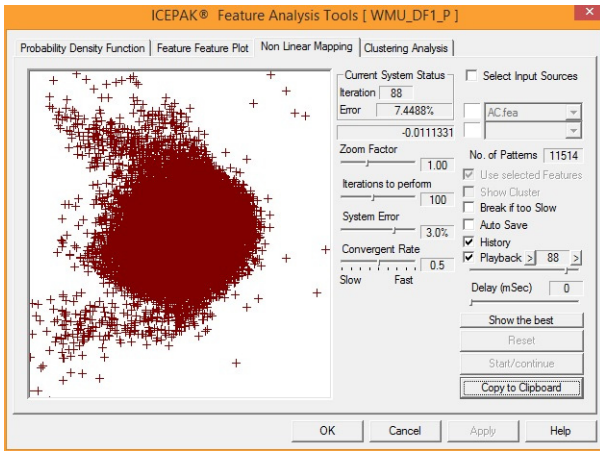


Figure 5-4. NLM Phase Domain

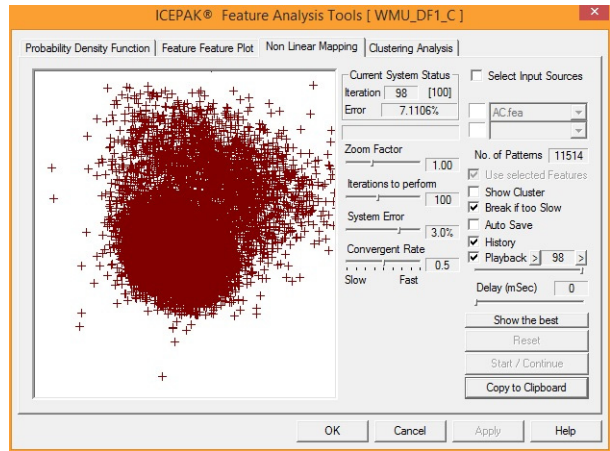


Figure 5-5. NLM Cepstral Domain

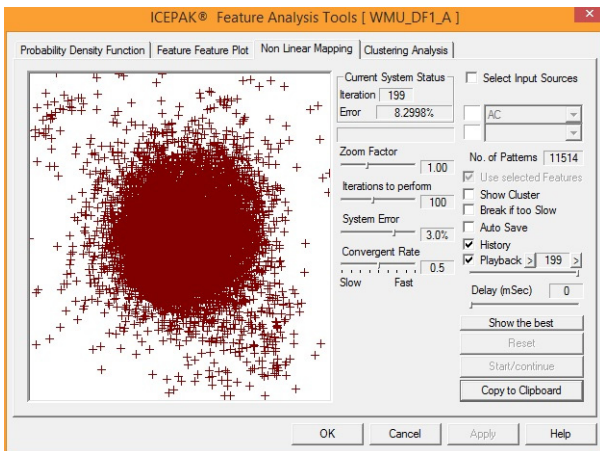


Figure 5-6. NLM Auto-Correlation Domain

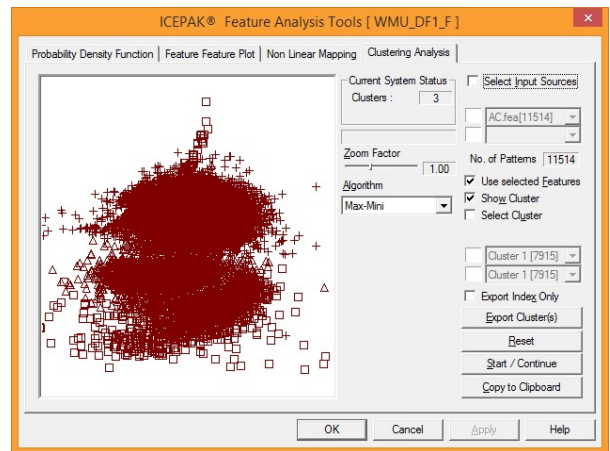


Figure 5-7. Clustering Power Domain

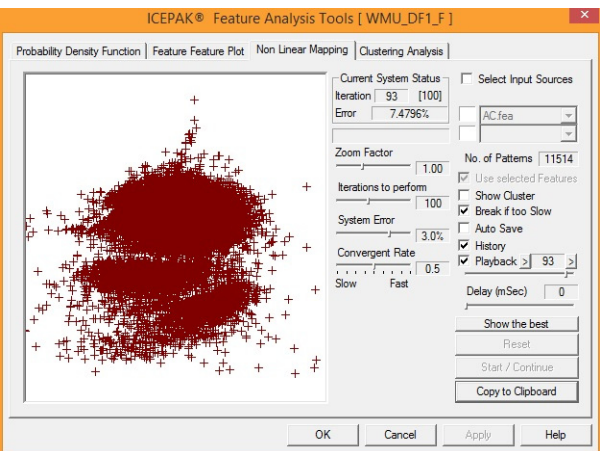


Figure 5-8. NLM Power Domain

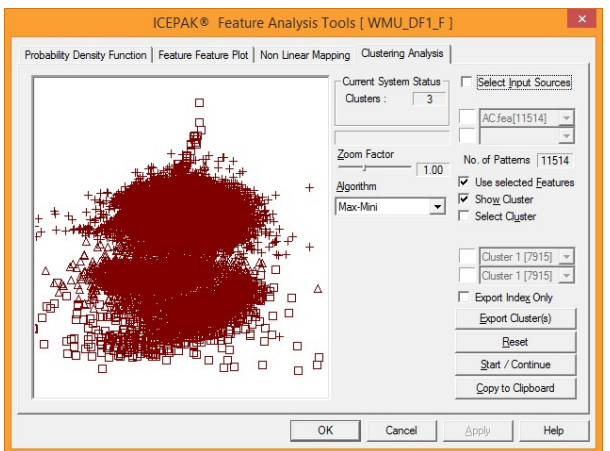
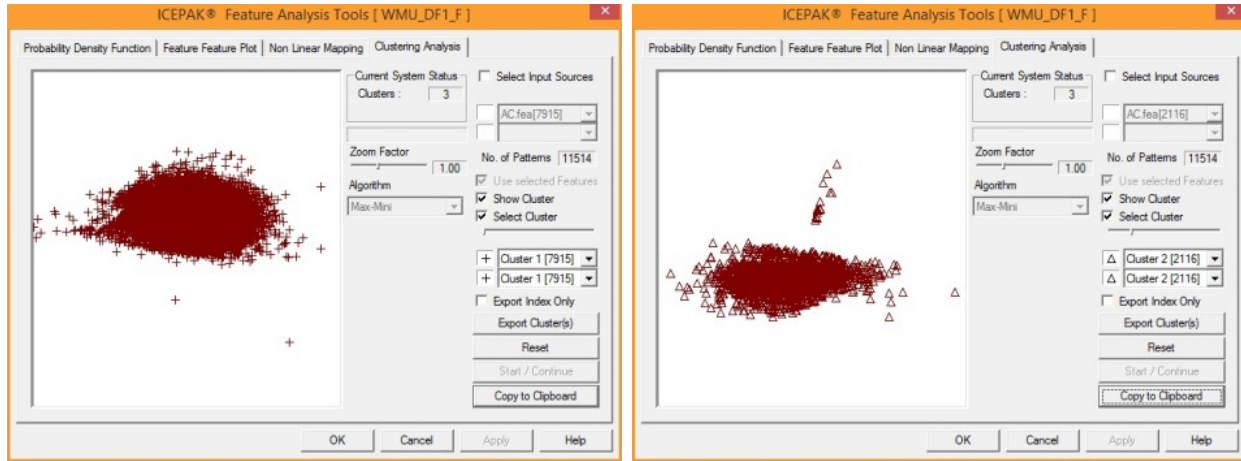
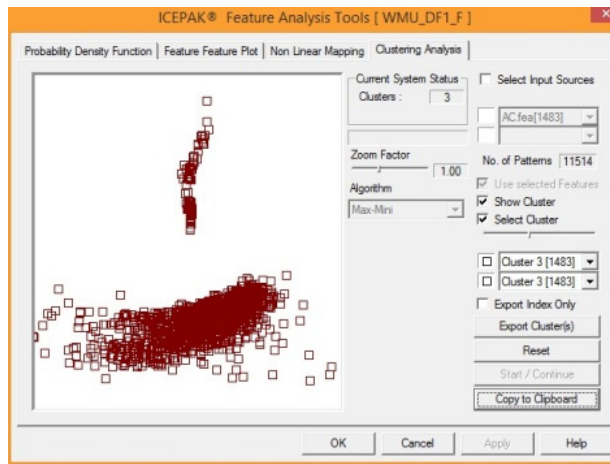


Figure 5-9. Clustering Power Domain



(a) Cluster 1

(b) Cluster 2



(c) Cluster 3

Figure 5-10. Individual data clusters

The individual data clusters were exported and labeled as [c11], [c12], and [c13]. Then, each cluster was used to train a three-class classifier. Four statistical classifiers (i.e., linear discriminant, K-nearest neighbor, empirical Bayesian, and minimum distance classifiers) and a neural network classifier were tested. The design of the classifiers included optimizing the feature sets. The design procedure included separating available data into two groups; one was used to train the classifiers and the other to test the performance of the classifiers. The classification results are shown in Figure 5-11 to Figure 5-15. As an example, [c11] had a total of 7,915 data points. This set was separated into two groups of 3,957 and 3,958 data points for training and testing, respectively. When the linear discriminant three-class classifier was trained with 3,957 data points, the data was classified into three classes with rejections. As shown in Figure 5-11, classes 1, 2, and 3 contain 3777, 2, and 0 data points with 178 rejections. The classification rate is 95.45%. In other words, 95.45% of the data in [c11] falls into class 1 (i.e.,

3,777/3,957 × 100). A similar process was employed for [c12] and [c13] data sets, and yielded classification rates of 94.99% and 95.95%, respectively. When all three data sets were considered, the linear discriminant three-class classifier yielded a weighted average classification rate of 95.43% for training (Figure 5-11). Overall, all the classification methods yielded very high classification rates for training as well as for testing.

Linear Discriminant Classification Results							
	Class	1	2	3	Reject	Total	Percent
c11.cxf	1	3777	2	0	178	3957	95.45%
c12.cxf	2	0	1005	5	48	1058	94.99%
c13.cxf	3	0	3	711	27	741	95.95%
Training : 95.43%							
	Class	1	2	3	Reject	Total	Percent
c11.cxf	1	3822	2	0	134	3958	96.56%
c12.cxf	2	0	995	6	57	1058	94.05%
c13.cxf	3	0	7	715	20	742	96.36%
Testing : 96.08%							

Figure 5-11. Linear Discriminant

K-Nearest Neighbors Classification Results							
	Class	1	2	3	Reject	Total	Percent
c11.cxf	1	3827	2	0	128	3957	96.71%
c12.cxf	2	98	900	23	37	1058	85.07%
c13.cxf	3	1	48	678	14	741	91.50%
Training : 93.90%							
	Class	1	2	3	Reject	Total	Percent
c11.cxf	1	3817	1	0	140	3958	96.44%
c12.cxf	2	116	883	19	40	1058	83.46%
c13.cxf	3	0	51	676	15	742	91.11%
Testing : 93.37%							

Figure 5-12. K-Nearest Neighbors

Empirical Bayesian Classification Results							
	Class	1	2	3	Reject	Total	Percent
c11.cxf	1	3758	11	0	188	3957	94.97%
c12.cxf	2	12	971	49	26	1058	91.78%
c13.cxf	3	0	6	702	33	741	94.74%
Training : 94.35%							
	Class	1	2	3	Reject	Total	Percent
c11.cxf	1	3767	7	0	184	3958	95.17%
c12.cxf	2	17	946	60	35	1058	89.41%
c13.cxf	3	0	7	705	30	742	95.01%
Testing : 94.10%							

Figure 5-13. Empirical Bayesian

Minimum Distance Classification Results							
	Class	1	2	3	Reject	Total	Percent
c11.cxf	1	3879	0	0	78	3957	98.03%
c12.cxf	2	2	1014	0	42	1058	95.84%
c13.cxf	3	0	0	730	11	741	98.52%
Training : 97.69%							
	Class	1	2	3	Reject	Total	Percent
c11.cxf	1	3887	0	0	71	3958	98.21%
c12.cxf	2	2	1011	0	45	1058	95.56%
c13.cxf	3	0	0	724	18	742	97.57%
Testing : 97.64%							

Figure 5-14. Minimum Distance

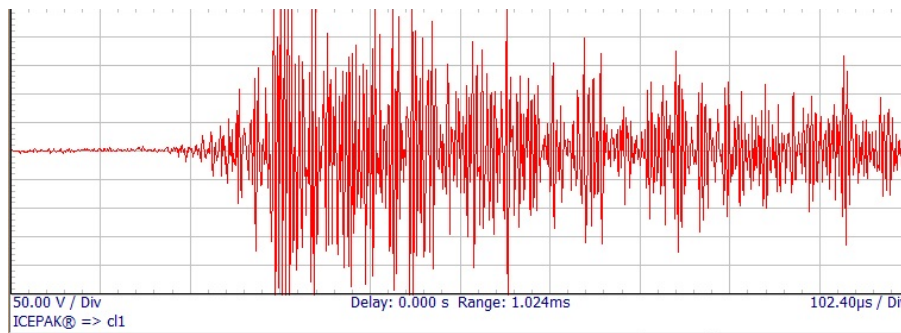
Neural Network Classification Results							
	Class	1	2	3	Reject	Total	Percent
c11.cxf	1	3846	0	0	111	3957	97.19%
c12.cxf	2	0	976	0	82	1058	92.25%
c13.cxf	3	0	48	667	26	741	90.01%
Training : 95.36%							
	Class	1	2	3	Reject	Total	Percent
c11.cxf	1	3856	0	0	102	3958	97.42%
c12.cxf	2	0	955	1	102	1058	90.26%
c13.cxf	3	0	55	667	20	742	89.89%
Testing : 95.14%							

Figure 5-15. Neural Network

Next, the PLB data was tested against this three-class classifier with a rejection option. The rejection option is triggered when an incoming signal cannot be classified with an acceptable level of confidence. The PLB data file contained 100 data points. The PLB data fell into class 1

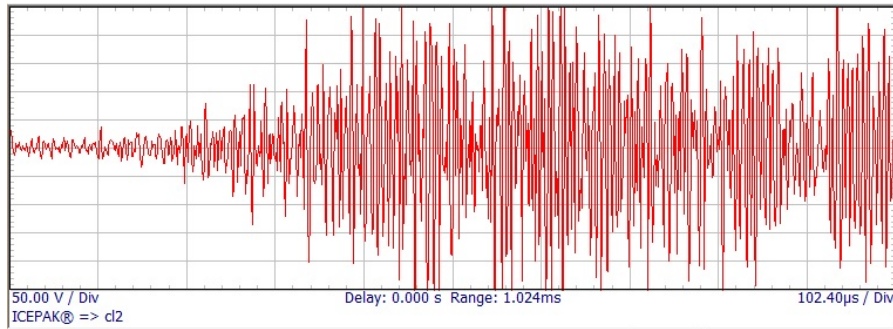
and 2 but not class 3, with a lot of rejections. Nine data points were classified as class 1 and 8 as class 2. None was classified as class 3. There were 83 rejections.

Finally, the trained classifiers and the associated feature extraction engine were exported from the ICEPAK™ program. The AE data collected from the bridge and PLB data were also exported in the PRISM-compatible waveform format. The PRISM program waveform visualization and real time classification capability were used to identify the type of waveforms in the three classifications (i.e., in class 1, 2, and 3) along with the rejected ones. Figure 5-16 to Figure 5-18 show sample PLB signal waveforms in class 1, class 2, and the rejected group.



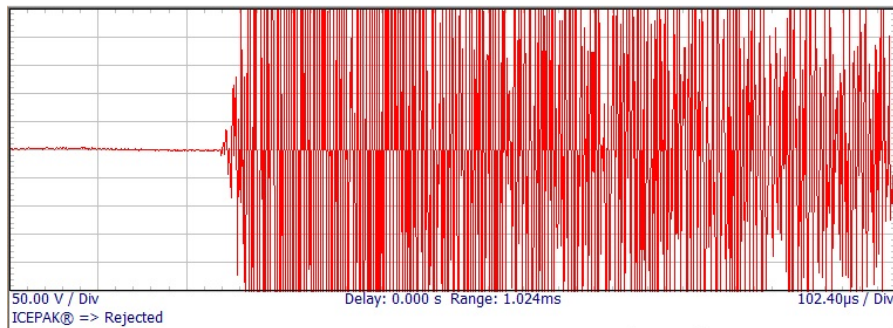
Note: X-axis: Time (102.4 μs/Div); Y-axis: Voltage (50 V/Div)

Figure 5-16. A sample PLB waveform in class 1



Note: X-axis: Time (102.4 μs/Div); Y-axis: Voltage (50 V/Div)

Figure 5-17. A sample PLB waveform in class 2

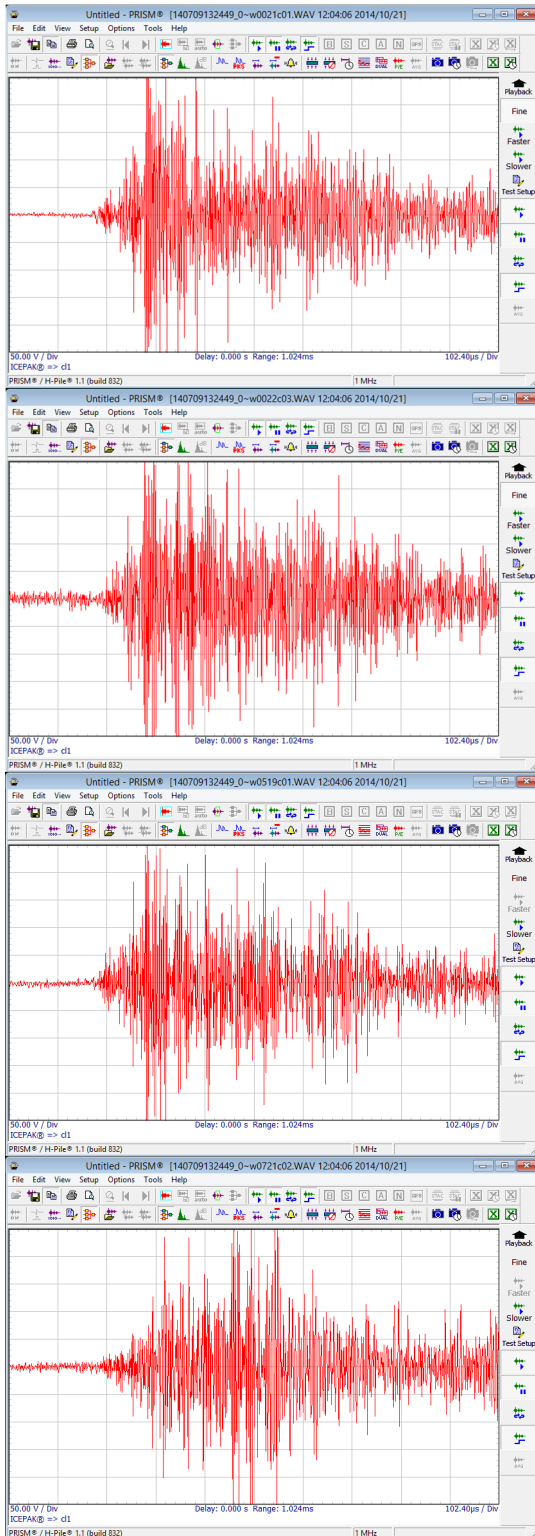


Note: X-axis: Time (102.4 μs/Div); Y-axis: Voltage (50 V/Div)

Figure 5-18. A sample rejected PLB waveform

The PRISM program was used to analyze the waveform characteristics of signals in each class and the rejected group, and yielded the following observations:

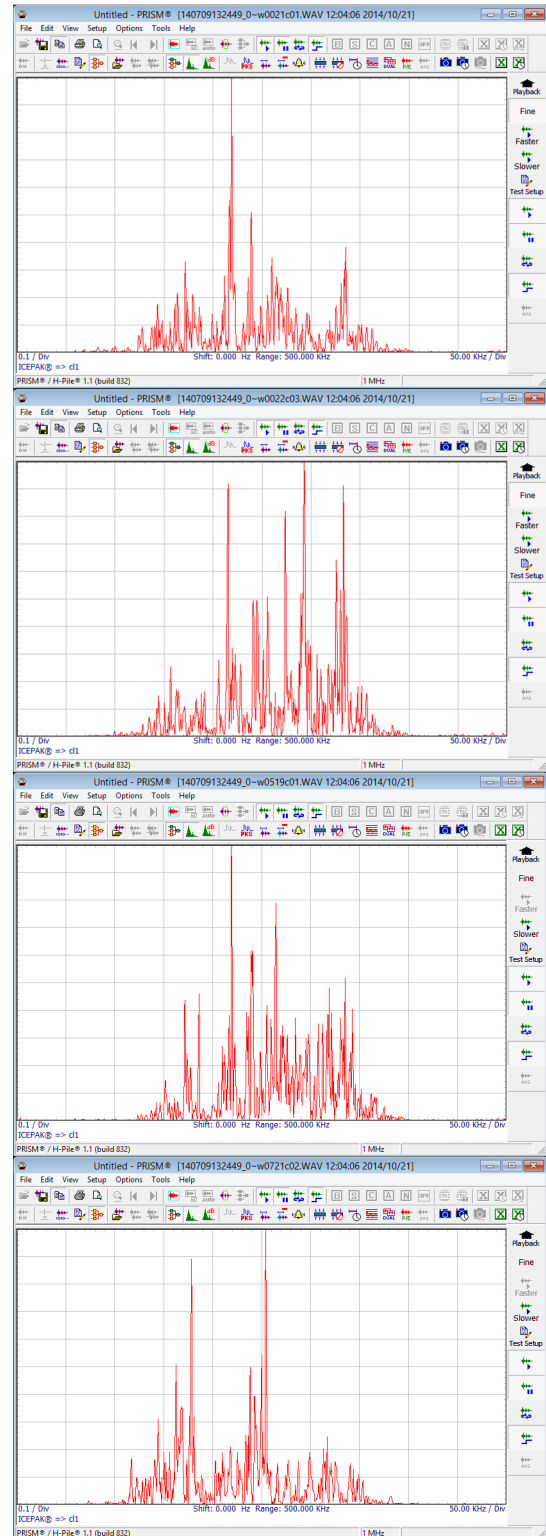
- The waveforms classified as class 1 usually have very fast rise times, relatively quiet pre-trigger portion, and a broad spectral content spanning from 100 to 400 kHz (Figure 5-19).
- The waveforms classified as class 2 usually have very fast rise times; however, the pre-trigger portion may show some small structure, and the main pocket contains multiple ringing peaks. The spectral content mainly centers around 150 kHz with very little or nothing above 250 kHz, and nothing below 100 kHz (Figure 5-20).
- The waveforms classified as class 3 usually have a slower rise time, and the spectral content is mainly located below 100 kHz and centered around 50 to 75 kHz. Moreover, there is absolutely nothing above 200 kHz (Figure 5-21).
- The waveforms classified as “rejected” are mostly associated with over-saturated clipped waveforms, and some have slow changing, somewhat smooth, waveform centered around 50 kHz (Figure 5-22).
- The number of waveforms being classified as class 1 is 4 to 6 times more than those of class 2 and class 3 while the sizes of class 2 and class 3 are relatively comparable. In general, there are about 5% of waveforms being rejected.



(a) Time domain

X-axis: Time (102.4 μ s/Div)

Y-axis: Voltage (50 V/Div)

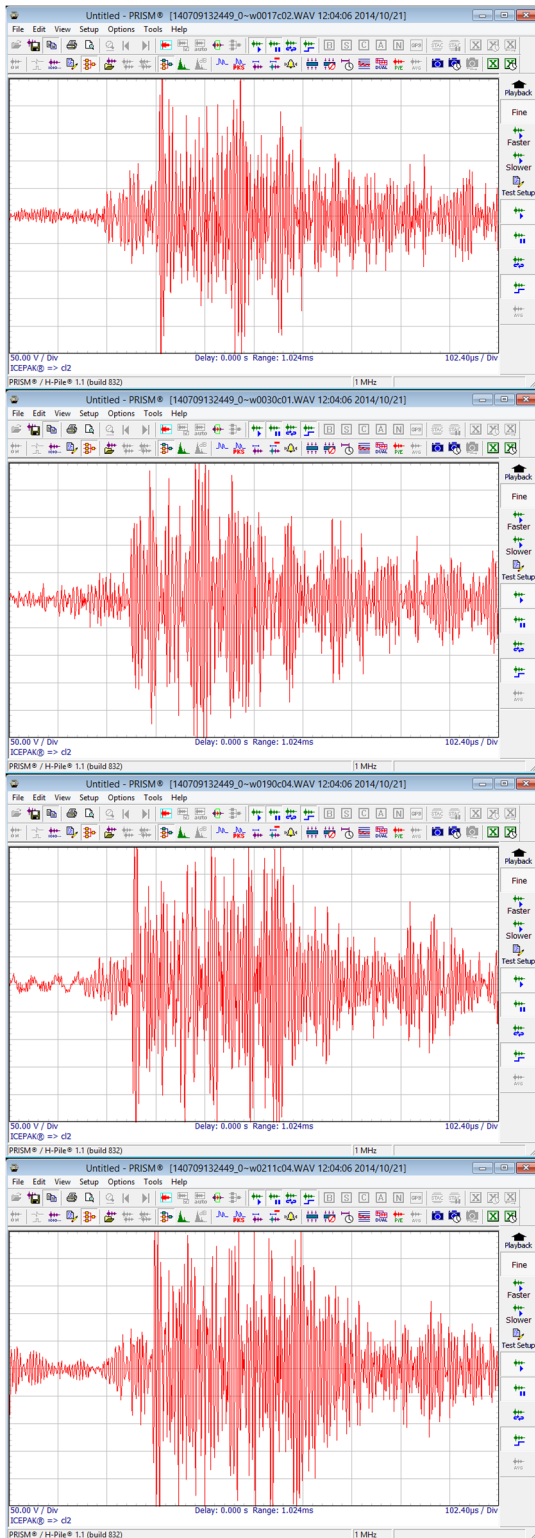


(b) Frequency domain

X-axis: Frequency (50 kHz/Div)

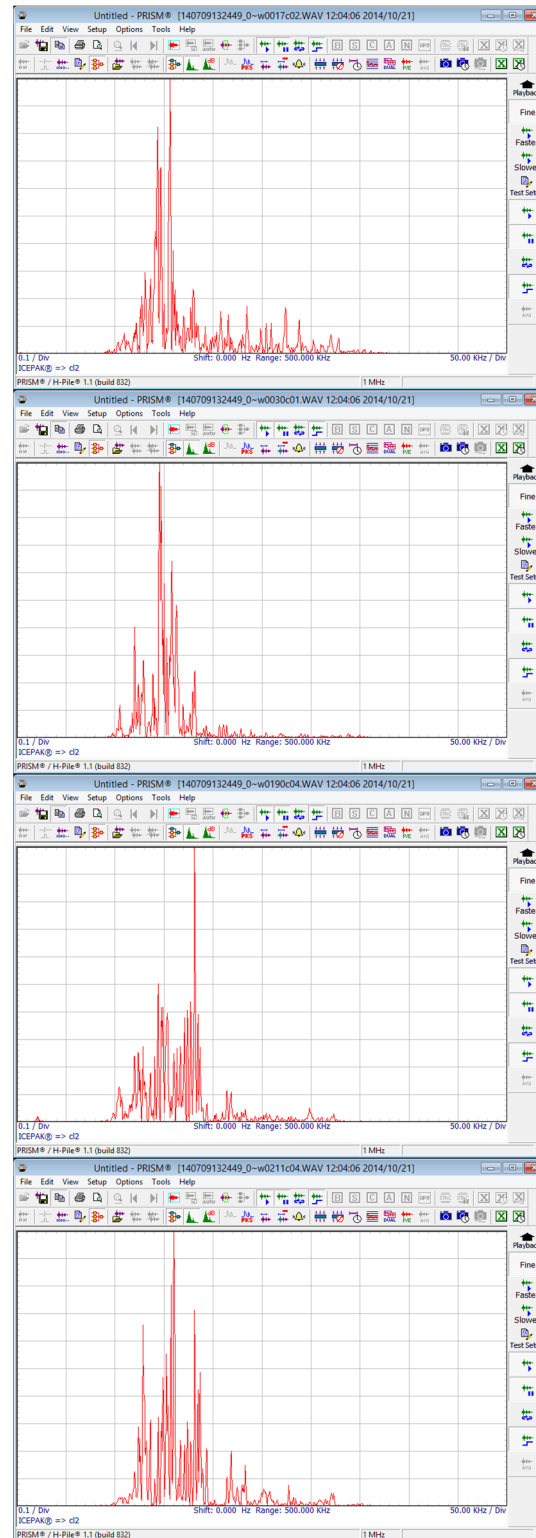
Y-axis: Amplitude (0.1/Div)

Figure 5-19. A sample class 1 waveform and its power spectrum



(a) Time domain

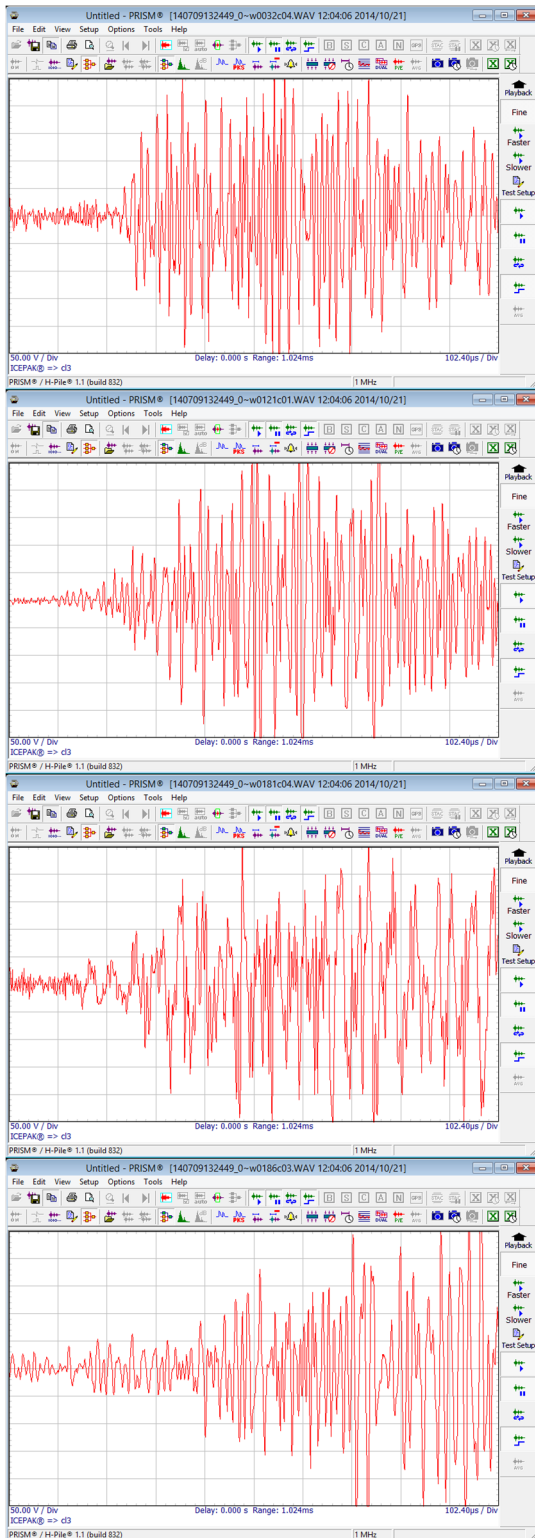
X-axis: Time (102.4 μ s/Div)
Y-axis: Voltage (50 V/Div)



(b) Frequency domain

X-axis: Frequency (50 kHz/Div)
Y-axis: Amplitude (0.1/Div)

Figure 5-20. A sample class 2 waveform and its power spectrum



(a) Time domain

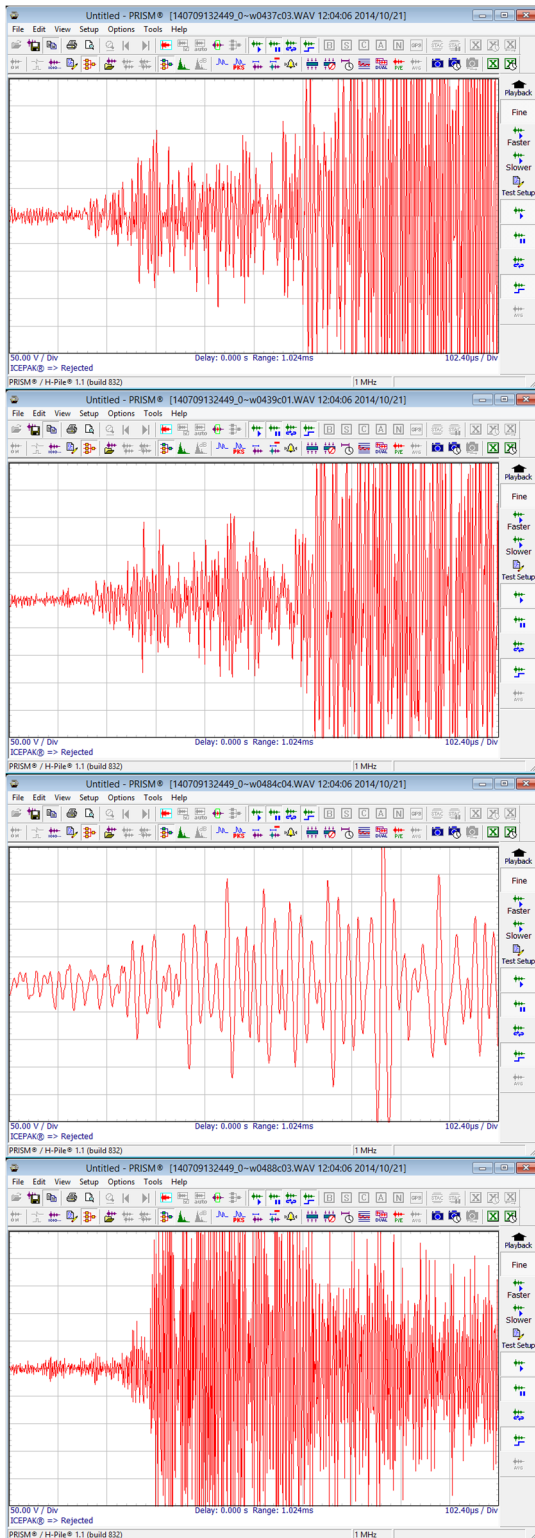
X-axis: Time (102.4 μ s/Div)
 Y-axis: Voltage (50 V/Div)



(b) Frequency domain

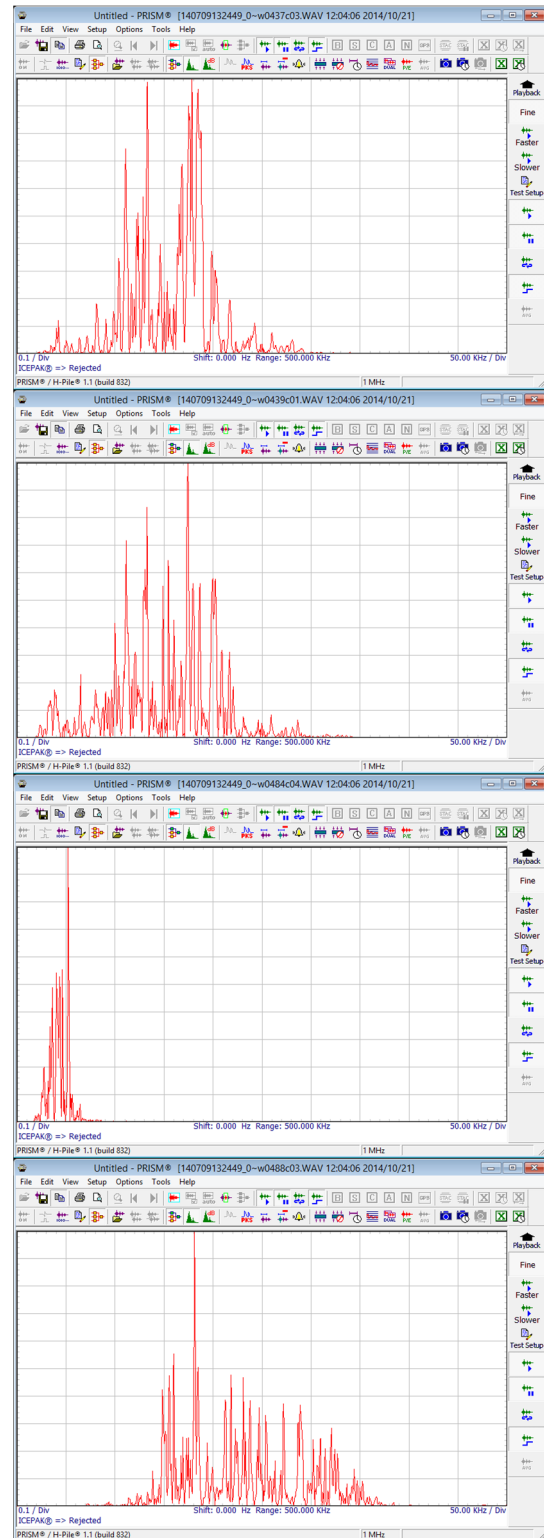
X-axis: Frequency (50 kHz/Div)
 Y-axis: Amplitude (0.1/Div)

Figure 5-21. A sample class 3 waveform and its power spectrum



(a) Time domain

X-axis: Time (102.4 μ s/Div)
 Y-axis: Voltage (50 V/Div)



(b) Frequency domain

X-axis: Frequency (50 kHz/Div)
 Y-axis: Amplitude (0.1/Div)

Figure 5-22. A sample “rejected” waveform and its power spectrum

5.1.5 AE Data Analysis Observations

There are two general types of fracture-related AE activities observed under cyclic loading conditions: crack tip opening during increased loading (upward load cycle) and crack face rubbing during decreasing load (downward cycle). This observation and correlation of the AE activities was derived largely based on past railroad bridge inspection experience of TISEC Inc.

The observations of sample data analysis show that both class 1 and class 2 waveforms are more structured with a faster rise time at the beginning of the waveform. Thus, they are associated with the AE signals from the crack opening. Even though class 1 and class 2 waveforms represent characteristics of crack opening signals, more accurate characterization requires having access to AE signals that represent properties of steel used in the bridge, component dimensions, exposure conditions, etc. Class 3 waveforms are more slowly rising, and their spectral content is more in line with common background transient noise. The rejected waveforms are more likely due to saturation and clipping of the signal, and the non-saturated ones, centered around 50 kHz are more likely results from structural resonance.

Since class 1 and 2 waveform characteristics closely represented AE signals from the crack opening, the source location plots were analyzed. As shown in Figure 5-23, there were no active sources documented within the zone of interest. Therefore, further analysis was not performed. When AE sources are located within the zone of interest, the following steps can be followed to validate the presence of potential cracking or crack opening events:

- Check the waveforms (Figure 5-24) to evaluate the resemblance of signals to the crack opening signals.
- Observe the source location plots for the formation of data clusters and the cluster growth direction.
- Correlate AE events with the strain data from the strain gage that is mounted to develop the load matrix. If AE events occur during increase in strain, there is a potential for the presence of a crack opening event.
- If the observations of the above steps require additional investigations, make a field visit and perform NDE to confirm the observations.
- If NDE fails to identify cracking, adjust signal thresholds and gains to calibrate the monitoring system for the specific detail.

5.2 FATIGUE PERFORMANCE EVALUATION

5.2.1 WIM Data and Hot Spot Stresses

WIM data was obtained for I-94 EB from a station located in Berrien County, City of New Buffalo. The station is located 22.5 miles west of the bridge site. The data covers 11 months of a year, except August due to a corrupted data file. According to the data, the bridge carries 48,500 vehicles daily, with 30% of the vehicles being trucks (i.e., ADTT of 14,550). Of the trucks, 84.6% travel in the outer lane (i.e., 12,309 trucks).

The gross weight of the fatigue truck was calculated following the Guide Specifications for Fatigue Evaluation of Existing Steel Bridges (AASHTO 1990), Section 2, Alternative 3, and weigh-in-motion data. Use of 11 month data yielded the gross weight of 57 kips. Following the AASHTO LRFD (2013) Article 3.6.1.4, an impact factor of 15% and a constant spacing of 30 ft between the main axles were used in analysis. As per the MBE (2011), 75 percent of the stress calculated using the fatigue truck with impact was used. Following the procedure discussed in section 3.6, fatigue truck load with impact was applied, and the weld toe stresses at L₁ web gap were calculated (Table 5-1). As per the MBE (2011) commentary C7.2.2.2, a multiplier less than two can be used to calculate the maximum stress range when the fatigue truck load is greater than 54 kips. However, a factor of two was considered to yield a conservative result. With the factor of two, the maximum stress range, $(\Delta f)_{max}$, ranges from 10.54 ksi to 10.88 ksi.

Table 5-1. HSS at L₁ Weld Toe due to Fatigue Truck Load

Reference point location from weld toe	Distance from weld toe with t = 0.545 in. (in.)	Stress in Y-direction (S _{YY}) (ksi)	
		Fixed Abutment	Pinned Abutment
0.4t *	0.218	3.75	3.87
0.9t	0.491	2.52	2.60
1.4t	0.763	2.03	2.10
*t = web thickness	Hot Spot Stress (ksi)	5.27	5.44

According to Hobbacher (2008), all applicable load effects need to be superimposed. Pook (2007) indicated that the residual stresses affect fatigue performance in the same manner as the mean applied stress. As presented in section 3.6.5.2, depending on the girder end fixity over the abutment, hot spot stress at the L₁ web gap due to cast-in-place concrete deck weight ranges from 6.57 ksi to 9.14 ksi. According to the statements presented in Hobbacher (2008) and Pook (2007), the fatigue evaluation of L₁ detail requires combining deck weight effects and the fatigue truck induced stress. Following the procedure discussed in section 2.3.4, hot spot stress and S-N

curves can be used to evaluate fatigue performance. The L₁ web gap detail is a Category C' detail with a constant-amplitude fatigue threshold (CAFT) of 12 ksi. As discussed in section 2.3.4, the use of S-N curve with hot spot stress for fatigue performance evaluation requires modifying the values using a hot spot stress ratio between reference detail and the detail to be assessed. In order to simplify the calculation procedure presented herein, the S-N curve and the CAFT values were used without any modifications. When the combined effect of cast-in-place deck load and the fatigue truck is considered, the maximum effective stress, $(\Delta f)_{\max}$, ranges from 17.11 ksi to 20.02 ksi. When compared with the CAFT of 12 ksi, the detail will have a finite fatigue life.

5.2.2 Hot Spot Stresses from Field Measured Strain Data

Three strain gages were mounted at the L₁ web gap to calculate weld toe stress (Figure 4-5). As per the hot spot stress calculation guidelines presented in Hobbacher (2008), the gages were mounted at a 0.4t, 0.9t, and 1.4t distance from the weld toe. In this particular instance, t is the thickness of the girder web. Figure 5-25, Figure 5-26, and Figure 5-27 show a set of sample strain data collected during the study. The strain data collected using each gage was multiplied by the steel modulus of elasticity, 29,000 ksi, to calculate the stresses at respective locations (i.e., $\sigma_{0.4t}$, $\sigma_{0.9t}$, and $\sigma_{1.4t}$). Then the hot spot stress (HSS) was calculated using Eq. 5-1 as a time series. The ASTM E1049-85 rainflow counting algorithm was used to calculate stress ranges and the respective number of stress cycles. Finally, the measured effective stress range, Δf , was calculated using Eq. 5-2.

$$2.52 \sigma_{0.4t} - 2.24 \sigma_{0.9t} + 0.72 \sigma_{1.4t} \quad (5-1)$$

$$\Delta f = (\sum \gamma_i \Delta f_i^3)^{\frac{1}{3}} \quad (5-2)$$

where, γ_i = fraction of cycles at a particular stress range and Δf_i = midwidth of the particular stress range.

According to the procedure given in MBE (2011), the effective stress is calculated using Eq. 5-3. When strain data is collected through field measurements and the mean fatigue life is to be calculated, the stress-range estimate partial load factor, R_s , is taken as 1.

$$(\Delta f)_{eff} = R_s (\sum \gamma_i \Delta f_i^3)^{\frac{1}{3}} \quad (5-3)$$

Section 7 of MBE (2011) notes that field measurements are the most accurate way to estimate the stresses acting on a bridge of interest; however, the maximum stress range is unlikely to be observed by collecting data within a limited duration. As a result, the MBE (2011) recommends using the maximum stress range of twice the measured stress range, i.e., $(\Delta f)_{\max} = 2(\Delta f)_{\text{eff}}$.

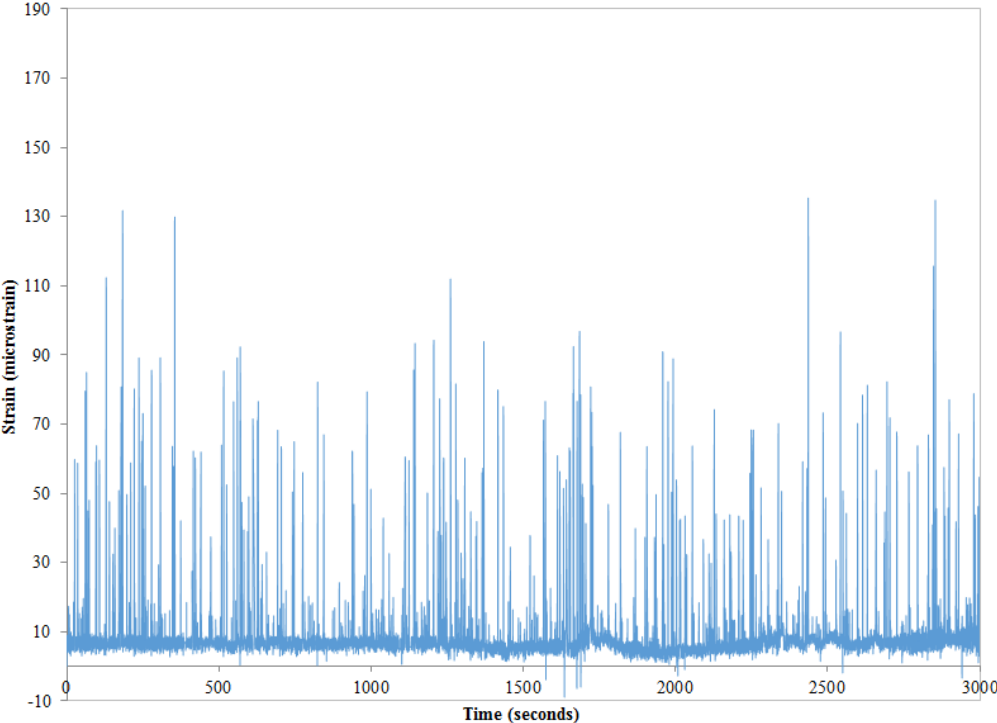


Figure 5-25. A sample strain profile collected at 0.4t

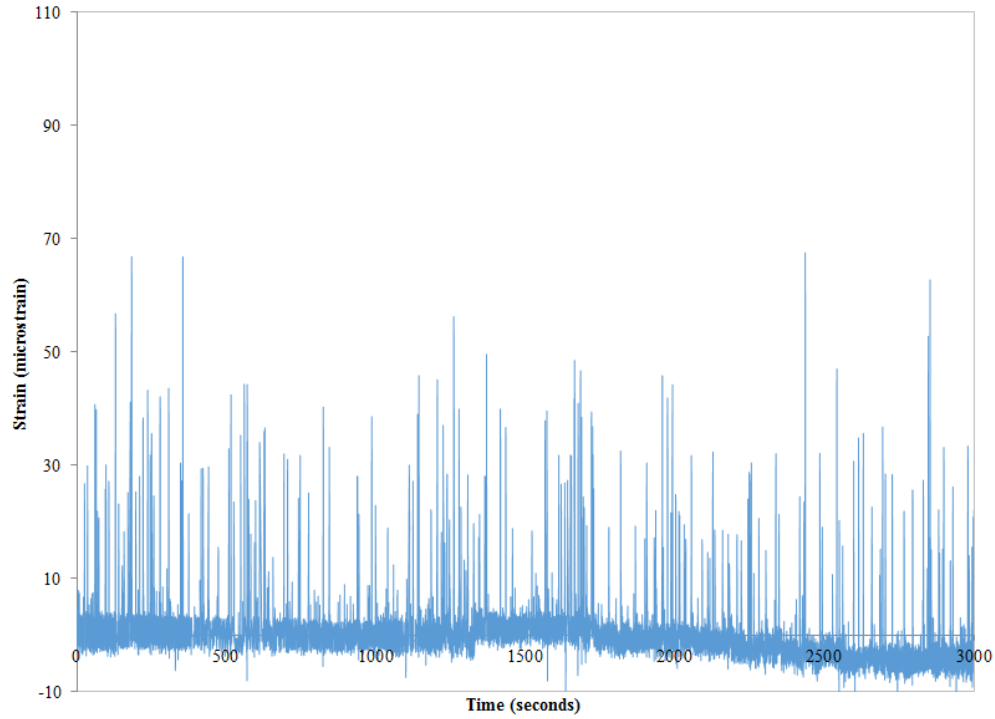


Figure 5-26. A sample strain profile collected at 0.9t

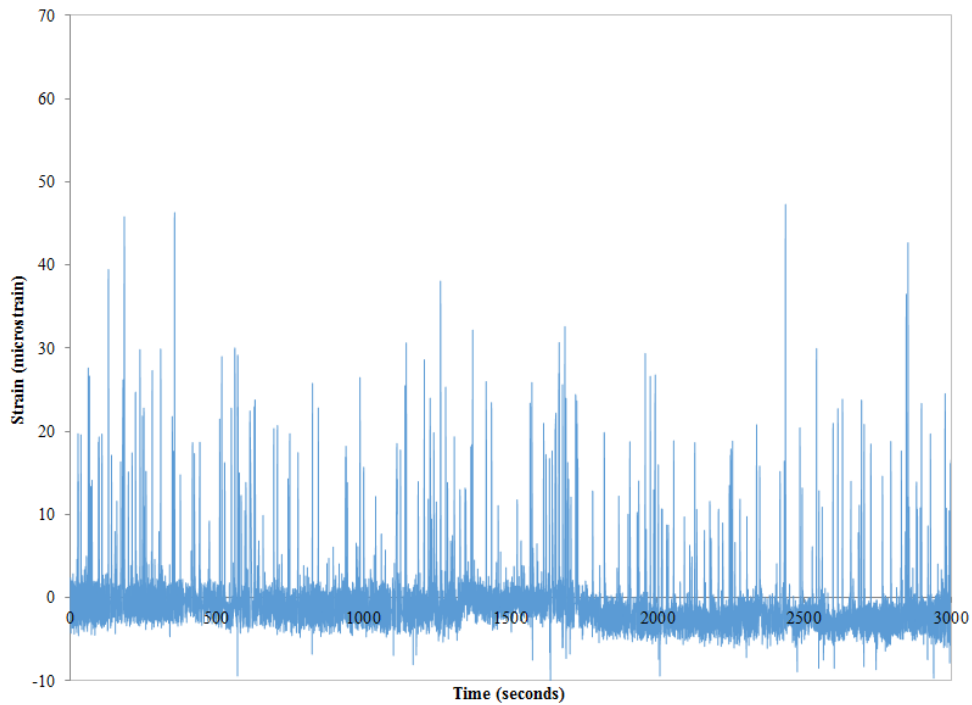


Figure 5-27. A sample strain profile collected at 1.4t

Hobbacher (2008) presented a procedure to use S-N curves with hot spot stresses (See Section 2.3.4 for details.) Even though hot spot stresses are used in this section for fatigue performance evaluation using measured strains, the S-N curve and the CAFT value of Category C' detail were

used without any modifications. Even if all the stress cycles are counted, the effective stress range, $(\Delta f)_{\text{eff}}$, calculated using strain data recorded at the web gap is only 0.8 ksi. As per the MBE (2011), the maximum stress range is 1.6 ksi, which is twice the effective stress range [i.e., $(\Delta f)_{\text{max}} = 2(\Delta f)_{\text{eff}} = 1.6$ ksi]. When the stresses induced by the cast-in-place deck dead load is included, the $(\Delta f)_{\text{max}}$ ranges from 12.14 ksi to 12.48 ksi, which is slightly greater than the CAFT of 12 ksi, and it can be safely assumed to have an infinite fatigue life. However, the maximum stress ranges calculated using strain data are much smaller than the stresses calculated using fatigue truck loads based on WIM data. Above all, the cast-in-place concrete deck weight has generated very high stresses at the weld toe and requires further investigations.

5.3 RELIABILITY PERFORMANCE OF THE MONITORING SYSTEM

5.3.1 AE and Strain Data Acquisition

As presented in section 4.1.1, the monitoring system has a low power computer with a single AE board and 4 AE sensors. Channel 1 of the AE board malfunctioned after one year and two weeks from system installation on the bridge. The Mistras Inc. had a one-year warranty for the system, and the board was repaired and tested as per the warranty terms even though the warranty time had briefly expired. The diagnostic report stated “*the dual ADC IC at location U14A failed, the part number 13.04840 was replaced, and then retested channel 1 and the other three channels for signal amplitude and noise levels.*” Other than the aforementioned channel 1 malfunction, the system was performing as expected.

The Mobile Broadband 5GB data plan from Verizon Wireless and Sierra Wireless – AirLink GX400 modem were used for communication and data transfer. The monitoring system is capable of acquiring strain data at a fast rate adequate to capture traffic-induced strain. However, real-time display of data from 12 strain gages and 4 AE data channels significantly slows down the display speed. The objective of this study was to monitor a targeted detail using a limited number of sensors. The real-time display of data from 4 AE sensors and the strain gage (for developing the load matrix) was satisfactory. Also, the delay in real-time display, wireless communication and data transfer speed is satisfactory.

5.3.2 Remote Access

LogMe In Pro software allows remote access and data transfer. Figure 5-28 shows a few menu options available in *LogMe In Pro*. *Remote Desktop Connection* can be used to access the remote computer in the SHM system. At several instances, operating *LogMe In Pro* features did not work due to an incompatibility between *LogMe In* and *Remote Desktop Connection*. When *LogMe In Pro* is activated following *Remote Desktop Connection*, the file transfer feature through *File Manager* becomes inactive. Further, once the *Remote Control* panel is accessed, a blank window opened and showed the message: “*Terminal Server Display is Inactive.*” This problem was rectified after restarting the system using the *Reboot* option available under the *Computer Management* pulldown menu in *Log Me In Pro*. At one time, the system was in operation but could not access using *Log Me In Pro*. Hence, *Remote Desktop Connection* was used and gave access to *Log Me In* technical support using the logmein123.com website. Technical support provided a code over the phone to enable the web access. The Pro version of *Log Me In* was installed remotely, and the system was rebooted using the rebooting program available on the desktop.

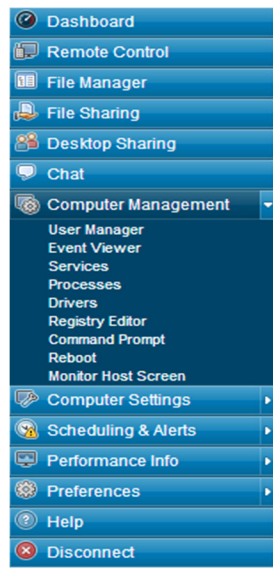


Figure 5-28. Menu options available in *LogMe In Pro*

5.3.3 Data Replay

AE Win can be used on a computer without an AE data acquisition board in the office to replay data downloaded from the remote monitoring system. When an AE board is not connected to the computer, the warning shown in Figure 5-29 appears. Once the “OK” button is selected, a

template file is loaded. If needed, the reasons for the warning can be viewed in the *error.log* file in the default folder. In order to replay data, a sensor layout file (*.lay) that is developed for the particular bridge needs to be opened before replaying the data file. At several instances, the software crashed, and the message shown in Figure 5-30 appeared. Sometimes, this problem was rectified by opening a default layout file before opening the user generated bridge specific layout file.

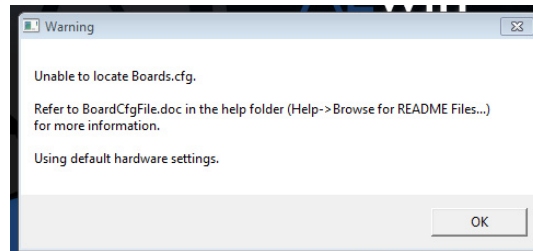


Figure 5-29. A warning message that appears when data replay program is opened

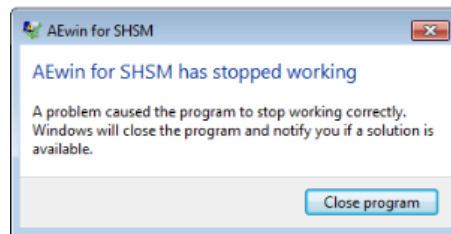


Figure 5-30. Program closure warning

5.3.4 System Reboot

As discussed in section 4.1.1, the computer should be rebooted using the rebooting program available on the desktop. It is very important to follow the rebooting sequence especially when the system is remotely located.

5.3.5 MS View

MS View program is used to display and record solar power system data (See section 4.1.5.3 for more details.) However, when the MPPT charge controller is programmed using *MS View*, it requires disconnecting and reconnecting the data cable manually from the computer in order to establish data communication. Otherwise, the MPPT charge controller is not identified by the *MS View* software. This requires programming the MPPT charge controller and evaluating the proper functioning of the device before incorporating the device in a remote monitoring system.

5.3.6 Solar Array

As the first step in solar power system performance evaluation, performance of the MPPT charge controller was evaluated under laboratory conditions using a constant voltage power supply. Figure 5-31 shows power supply (array) voltage, battery voltage, charge current, and load current. Initially, a load (other than the monitoring system) was connected and allowed to drain charge from the battery without supplying power from the array. As shown, the load drains a constant current of 1.70 A while the battery voltage drops steadily. When the battery voltage is about 11.8 V, array voltage was increased up to 17.4 V, and the charging cycle was started. As soon as the charging cycle started, there was an increase in battery voltage. The battery voltage was steadily increased to 14 V while the current drawn by the load was retained at 1.70 A. Once the battery voltage reached the preset maximum of 14 V, the absorption stage of the charging cycle began, and the battery voltage was maintained. When the battery voltage reached the maximum, there was an artificial increase in array voltage, but the charge current decreased. During the absorption duration, the charge current dropped gradually until it reached the load current of 1.70 A. The charge current and the load current remained at this value as long as the array voltage is maintained at a voltage above the battery voltage.

A typical discharge, charge, absorption, and float cycles are shown in Figure 5-32. During laboratory testing, the float cycle was not observed even after 5.5 hours. Also, when the power supply (array) voltage was disconnected, a sudden drop in battery voltage was observed (Figure 5-32).

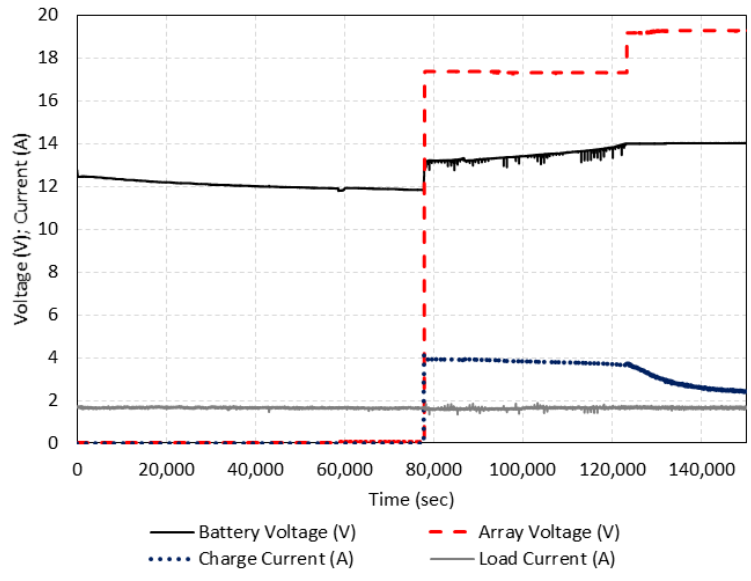


Figure 5-31. Battery charging and discharging evaluation under laboratory conditions

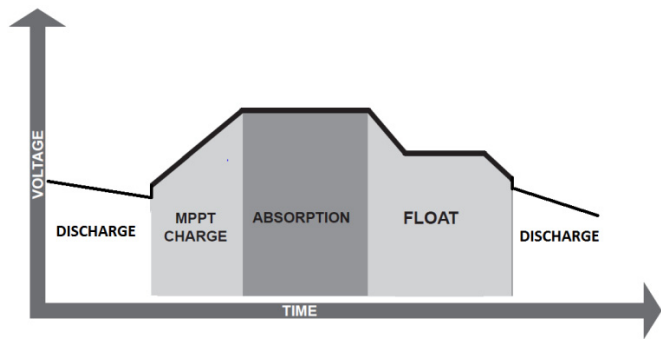


Figure 5-32. Theoretical battery discharge and recharge cycle

The solar array system performance was evaluated under field conditions. The data logging capability of the MPPT charge controller enabled the measurement of array voltage, array power, battery voltage, charge current, load current, exposure condition, and several other parameters. The solar power system performance was evaluated during the month of July, 2014. During the system evaluation period, the charge controller provided an average gain of 19% to the current produced by the solar panel, with peaks in current gain during peak sunshine hours of 34%. This average gain was lower than expected, but it was well within the range of 10% to 35% recorded in the operational manual. By knowing array power and voltage, the charge produced by the array was calculated (i.e., array power/array voltage). Experiments conducted under laboratory conditions showed negligible losses during power conversion (i.e., Power In \cong Power Out). Hence, by knowing the charge current recorded by the software and the array power, charge voltage is calculated (i.e., array power/charge current). Figure 5-33 shows recorded array

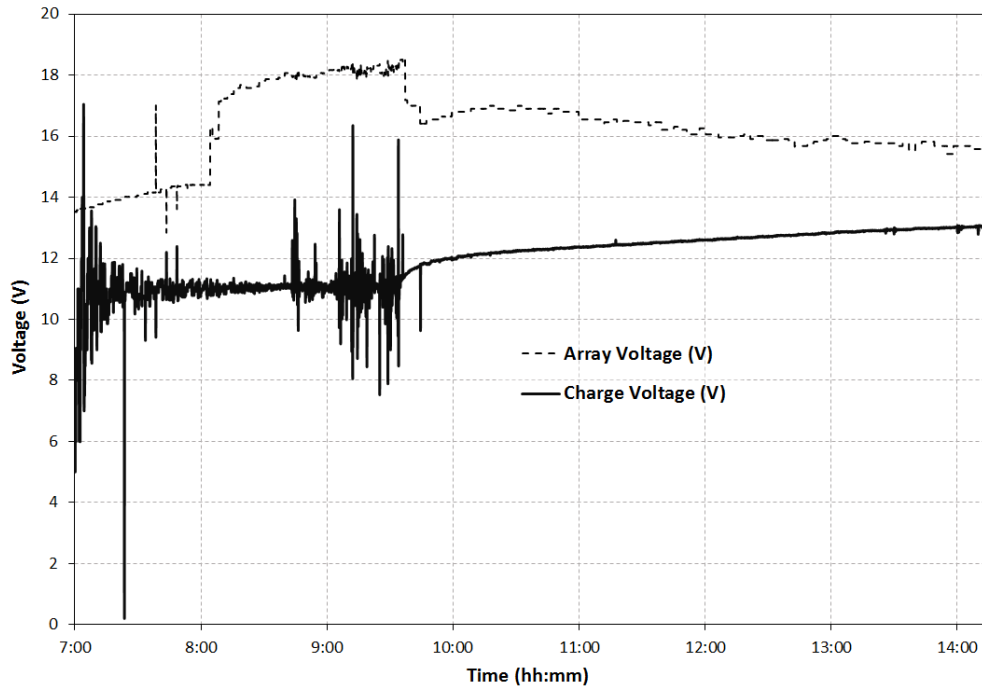
voltage and charge current as well as the calculated charge voltage and array current. Figure 5-33 shows the ability of the MPPT charge controller to increase the charge current to yield a greater efficiency in charging a battery.

The MPPT LVR and LVD thresholds were set to 13.6 V and 11 V, respectively. The targeted maximum battery voltage was set to 14 V. During this evaluation, absorption period in the battery charging cycle was not included. Hence, as soon as the targeted voltage of 14V was reached, the charge current supply to the battery was automatically disconnected from the charge controller. The objective was to check if the power supply was going to resume once the battery voltage drops but before reaching the LVD. Figure 5-34 shows the variation of battery voltage (V) and array voltage (V) during a typical day. As shown in the figure, during the period A (2 hours) and B (5.5 hours), the battery bank was not efficiently charged even if the array voltage was higher than the battery voltage. Figure 5-35 shows a repeat of similar charge and discharge cycles during more than 4 consecutive days of operation. The performance could have increased by including absorption period in the charging cycle as long as the array voltage remained at a value greater than the battery voltage (Figure 5-31 and Figure 5-32).

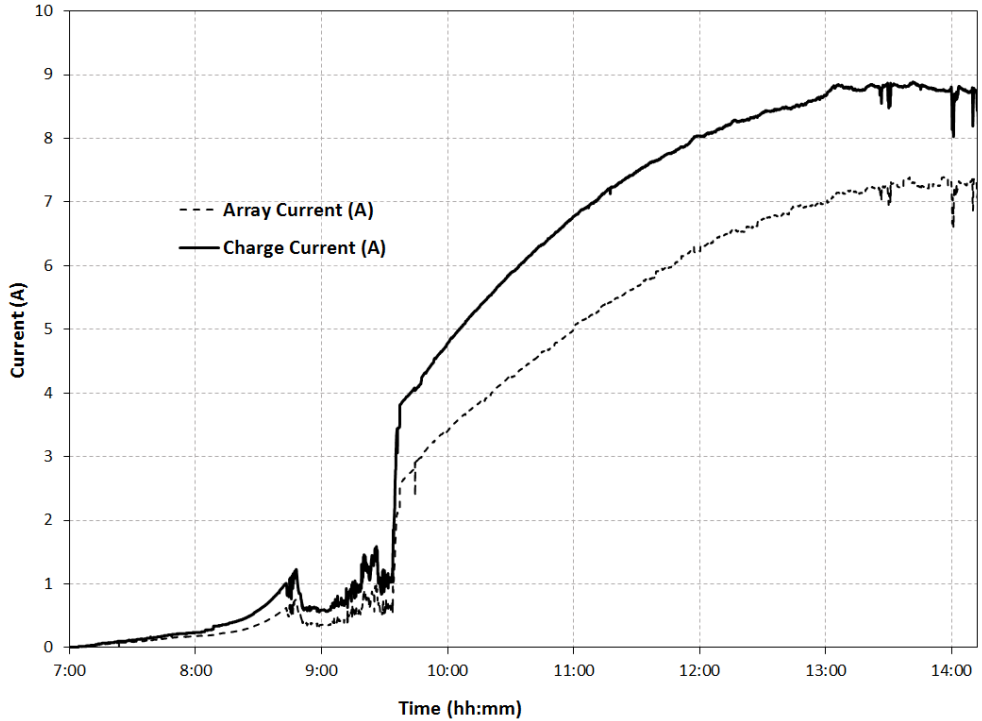
As shown in Figure 5-35, the charge controller was not able to charge the battery bank to up to 14 V. The observed maximums were 13.78 V (July 1), 13.56 V (July 2), 13.59 V (July 3), and 13.33 V (July 4). The observed lower voltages were 11.61 V (July 1), 11.39 V (July 2), 11.27 V (July 3), and 11.16 V (July 4). Even though it is not documented in the user manual, the data recorded during this evaluation shows that there is a relation between LVD and the restart of the battery charging cycle. Because of these reasons, once the maximum battery voltage is reached, the charge controller does not charge batteries to keep at the maximum voltage even if adequate power is harvested by the panels.

According to the data collected under specific site conditions with an average solar insolation of 5.85 kWh/m² per day in the month of July, the total charge harvested by the 140 W array was 50.8 A-hrs/day. In addition to the solar array efficiency, the MPPT charge controller efficiency also contributed to yield a 50.8 A charge. During the same period that the array was harvesting solar energy and charging the batteries; the load consumed was 30 A-hrs. Hence, only 20 A-hrs were remaining to operate the load when the panel was not harvesting energy. During that time,

the monitoring system (the load) consumed an average charge of 2.35 A. Hence, without any losses, the maximum duration that the system can operate using the remaining 20 A-hrs is 8.5 hrs ($20 \text{ A-hrs} / 2.35 \text{ A}$). Hence, in order to continuously operate a system that draws 2.35A under varying exposure conditions during summer requires a larger solar array, an extended battery bank, and exploring the optimum settings of the MPPT charge controller to use solar energy efficiently. In a nutshell, a solar power system needs to be designed based on the power demand, duration of monitoring, expected duration for power storage, time of the year, site location (latitude and longitude), and other site specific parameters that will reduce solar exposure on the panel. Therefore, the time of year and site location are two critical parameters in the design of a solar power system. As an example, the National Renewable Energy Laboratory (NREL 2014) presents the photovoltaic (PV) solar radiation data, and southwest Michigan receives solar radiation of about $2 \text{ kWh/m}^2/\text{day}$ during December and January while it is about $4.5 - 5.5 \text{ kWh/m}^2/\text{day}$ during July and August. Further, the ambient temperature during December/January falls well below freezing. Under such exposure conditions, battery power output drops to about 60% of its capacity. Similarly, if the battery temperature is about 95°F , battery service life is reduced by half. Therefore, solar array capacity needs to be sized based on the solar radiation while the battery bank needs to be sized by considering the exposure condition in addition to all other requirements.



(a) Variation of array voltage and charge voltage during a charging period



(b) Variation of array current and charge current during a charging period

Figure 5-33. Variation of array voltage, charge voltage, array current, and charge current during battery charging period

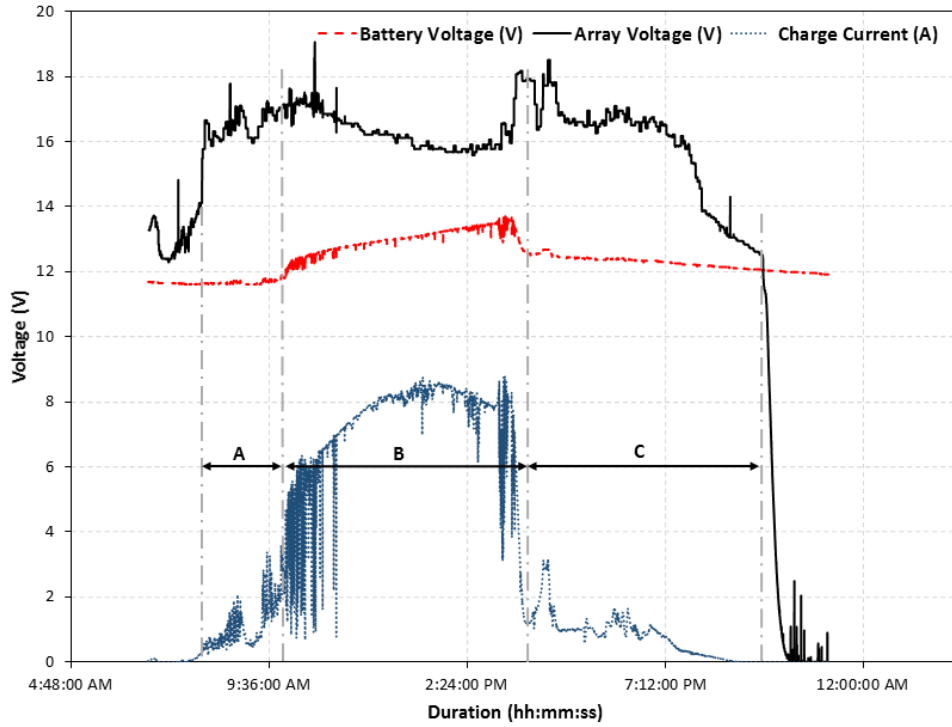


Figure 5-34. Variation of battery voltage and array voltage during a typical day

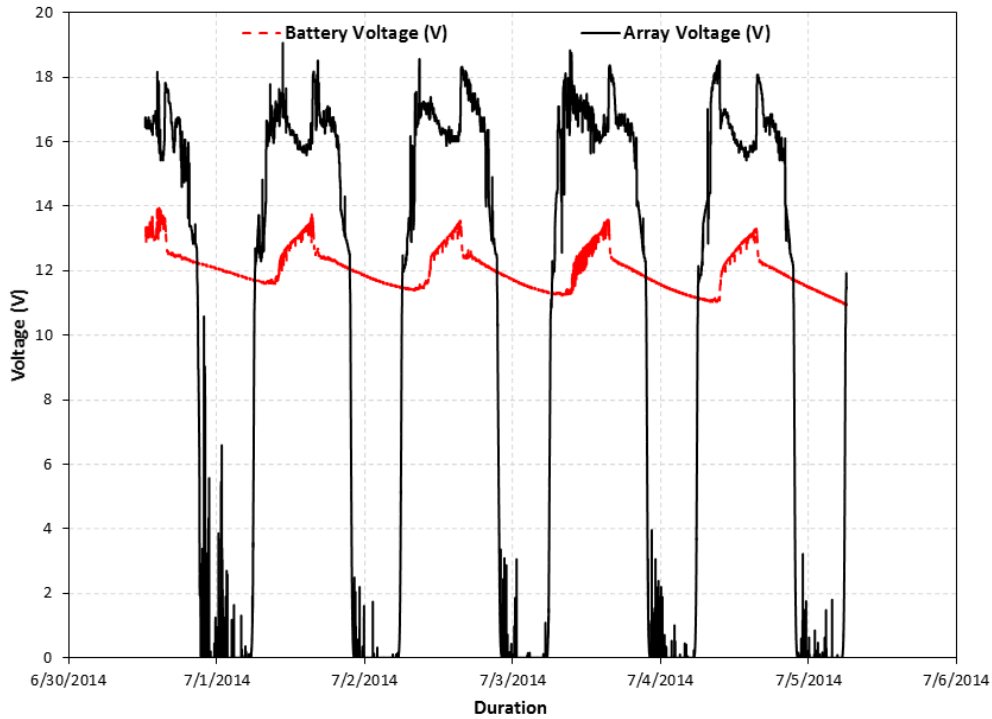


Figure 5-35. Variation of battery voltage and array voltage during continuous operation of a load from June 30 (12:21:38 hr) to July 5 (06:09:58 hr), 2014

5.4 SUMMARY

The following conclusions can be derived from the AE data analysis, fatigue performance evaluation, and monitoring system performance evaluation presented in this chapter:

- The data analysis methods presented in this section provides a sound basis for the use of acoustic emission (AE) for monitoring the condition of fatigue-sensitive details and/or retrofits. With a large database generated from operating traffic, tools for identifying and separating fracture events from traffic and ambient noise with a high recognition rate are provided. In addition, the associated theoretical basis is presented for providing the underlying concepts and assumptions.
- Examination of the overall AE data provides a basis for adjustment of the data acquisition parameters such as gain and threshold. While the PLB signals performed their role in confirming the source location capability, their oversaturation suggests that the gain can be reduced, and the threshold is adjusted accordingly to reduce the overall volume of the data.
- The effective stress that was calculated using the fatigue truck based on WIM data and field measured strains shows a significant difference. High stress ranges from the analytical calculations using the WIM data were obtained whereas the actual monitored stress ranges were much lower. This finding highlights the need of developing a comprehensive monitoring program for evaluating performance of fatigue-sensitive details especially when major decisions such as costly repairs, retrofits, and load postings are to be made.
- The monitoring system was subjected to outdoor environmental conditions during a period of more than a year. During this period, one of the AE channels was malfunctioned and repaired. A few software compatibility issues were encountered and resolved. In general, the performance of the monitoring system and associated software has been satisfactory.

6 SUMMARY, CONCLUSIONS, AND IMPLEMENTATION RECOMMENDATIONS

6.1 SUMMARY AND CONCLUSIONS

Fatigue is one of the most critical problems for steel bridges as well as for any steel structures that needs to be considered during design and operation. Fatigue cracking is developed at certain steel bridge details due to a direct result of the loads (load-induced fatigue) or a deformation that is not accounted for during design (distortion-induced fatigue). The details that are prone to load-induced fatigue can be identified using the detail categories presented in the AASHTO LRFD (2013) specifications, Table 6.6.1.2.3-1. Identifying the details that are prone to distortion-induced fatigue cracking requires a combined effort of utilizing information in bridge files, refined analysis, and experience. Developing high-fidelity analysis models is vital to identify details that are susceptible to distortion-induced fatigue, evaluate the causes of cracking or potential for cracking, estimate remaining life of details that are prone to distortion-induced fatigue, and to develop guidelines for instrumentation and monitoring.

MDOT performs inspections of over 200 bridges with fatigue-sensitive details, and was interested in identifying technology that can be implemented to evaluate performance of fatigue-sensitive details and retrofits. By considering MDOT monitoring needs and the vital role of refined analysis, this study was organized into five tasks. While the outcome of the fifth task is presented in Section 6.2, the other four tasks and the findings are described below.

(1) Review the state-of-the-art and practice literature to identify technologies for a structural health monitoring (SHM) system:

Technology for fatigue-sensitive detail monitoring, technology implementation considerations, and retrofit methods for fatigue-sensitive details were reviewed. After evaluating the needs and the state-of-the-art technology, an acoustic emission (AE) monitoring system with strain gages was recommended to be one of the most effective technology for fatigue event detection (i.e., crack initiation or crack growth monitoring). AE has been successfully implemented in the field and evaluated for continuous monitoring of fatigue-sensitive details. At this time, AE is the only technology that is capable of real-time monitoring of fatigue events and providing data for damage location detection. In addition to

the AE sensors, strain gauges are required to evaluate the stress state to calculate the remaining fatigue life, and to support AE data analysis by developing a load matrix.

(2) Select a bridge and perform structural analysis to identify details for monitoring:

The bridge (S16 of 11015) that carries I-94 EB over Puetz Road, located in Stevensville, Michigan, was selected for system implementation and performance evaluation. After reviewing MDOT biennial inspection reports and conducting a field visit to document bridge superstructure and substructure condition, the 54.5° skew and 56 ft - 6 in. long span was selected. The span consists of category C' fatigue-sensitive partial depth diaphragm details and a category E fatigue-sensitive welded cover plate detail. A 3D finite element model of the bridge was developed, and hot spot stresses were calculated under Michigan legal loads and deck dead load. Based on the analysis results, two web gap details that are located underneath the tuck lane were selected for instrumentation.

(3) Procure an SHM system:

As a commercially available implementation-ready SHM system, the TISEC SABRE™ system comprising the Mistras Group Inc. Sensor Highway™ II System instrumentation and a set of TISEC software post processing modules were selected as the basic AE system. One web gap detail was instrumented with 4 AE sensors and a strain gage while the other detail was instrumented with strain gages to calculate hot spot stresses.

(4) Install and calibrate the system, and analyze data:

The SHM system was installed, calibrated using pencil lead break (PLB) signals, and operated by powering through a solar power system. Many challenges are documented in the literature regarding AE data analysis and results interpretation. The following steps were followed during this study to analyze and interpret the AE data collected by the monitoring system:

- Selected an AE data set with signals exceeding a set threshold.
- Performed nonlinear mapping (NLM) using one feature domain at a time in the time, power, phase, cepstral and auto-correlation domains to visually detect significant naturally forming data clusters. (*Note: During this study, out of the 5 domains, the spectral power domain produced three significant clusters.*)

- Performed clustering with the same spectral power domain features. (*Note: Observed formation of three distinct clusters. These clusters were well aligned with the visual presentation of the NLM result. These observations confirmed the observations of NLM results.*)
- Separated the AE data set into three distinct clusters based on NLM and clustering analysis results.
- Classified each cluster using statistical and neural network classification methods, and selected the data belonging to each class for further analysis. (*Note: Use half of each cluster for training and the other half for testing the classification algorithms. All the classifiers yielded very high classification rates.*)
- Observed waveform characteristics in time and frequency domains to identify the class of signals that resemble the characteristics of signals that emanate due to fatigue events (i.e., crack opening) as well as the signals due to structural resonance and background noise.
- Developed conclusions based on observed signal characteristics, data presented in the source location plots, and experience.

Even though a large number of AE data sets were recorded during monitoring, data analysis and interpretation process followed during this study confirmed the nonexistence of the fatigue cracks at the monitored detail. With a large volume of data generated from operating traffic, tools for identifying and separating fracture events from traffic and ambient noise with a high recognition rate are provided; and the associated theoretical basis is presented. The signal types belonging to each class can be identified by inspecting the waveform features. Therefore, the data analysis capabilities presented during this study provides a sound basis for the use of AE for monitoring the performance of fatigue-sensitive details and elements or sections with retrofits.

Fatigue performance of a welded web gap detail was evaluated using (a) hot spot stress calculated using a finite element model loaded with a fatigue truck and (b) strain data collected using instrumentation. The gross weight of the fatigue truck was calculated as 57 kips using WIM data. Hot spot stress was calculated using a refined finite element model as per the guidelines presented by the International Institute of Welding (IIW). The maximum stress range at the weld toe was as high as 10.88 ksi. When combined with the other load effects, the stress range well exceeded the constant-amplitude fatigue threshold (CAFT) indicating a finite fatigue

life for the detail. The detail was instrumented with strain gages, and hot spot stress was calculated. The maximum stress range of 1.6 ksi was calculated using measured strain under ambient traffic. When combined with the effects of other loads, the maximum stress range barely reaches the CAFT indicating infinite fatigue life for the detail.

The monitoring system's ruggedness and reliability was evaluated by installing it on a bridge and subjecting it to severe outdoor exposure during a period of more than a year. During this period, one of the channels in the AE board malfunctioned, and was repaired. Minor issues were experienced with the real-time data display and software compatibility. However, within the data acquisition, interpretation, and presentation stream, these issues were resolved for this application. In general, the performance of the monitoring system and associated software is satisfactory.

6.2 IMPLEMENTATION RECOMMENDATIONS

After carefully evaluating the outcome of the four tasks, a two-tier implementation process is recommended as shown in Figure 6-1. Tier I includes assessment of bridges with repaired details. The first step is to identify the causes of cracking at the fatigue sensitive details through analysis and monitoring. At the same time, the monitoring data and analysis techniques can be used to evaluate the performance of the repairs and to develop necessary modifications to the structure and the detail to enhance the fatigue performance. Finally, the best performing retrofits can be identified for implementation in similar structures.

Tier II includes grouping bridges with fatigue-sensitive details based on defined attributes, and selecting a representative bridge from each group. Then, the fatigue serviceability index (Q) is calculated using refined analysis and a fatigue truck load. If $Q > 0.2$, routine inspections is performed. Otherwise, strains and fatigue events are monitored with two objectives: (1) to determine the presence of active fatigue cracks, and (2) to calculate Q using measured strains. The monitoring results are used to make repair, retrofit, or inspection decisions.

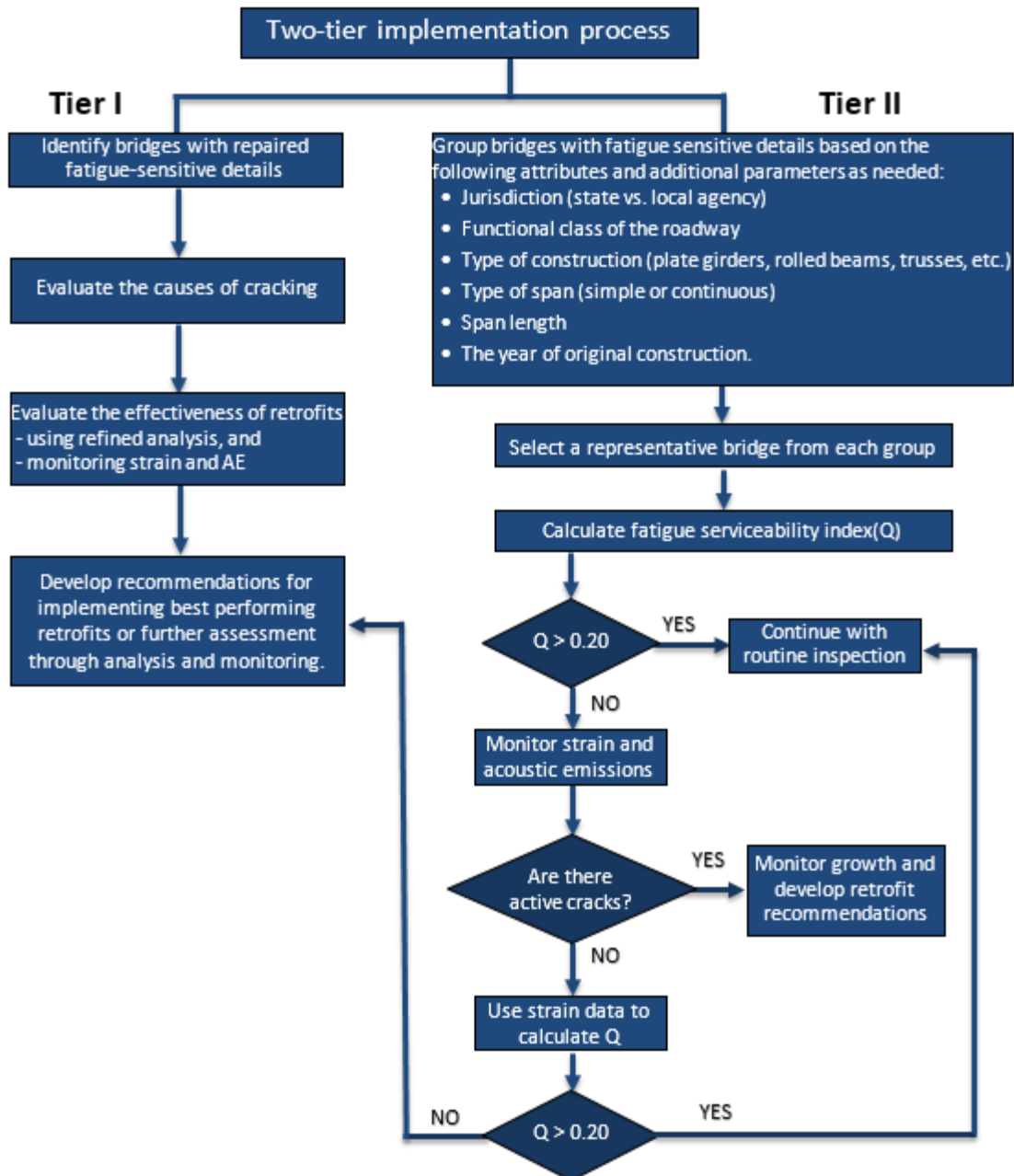


Figure 6-1. Two-tier implementation process

Additional recommendations to enhance the two-tier implementation process as well as for future research are listed below;

1. With ICEPACK, AE data interpretation capability was demonstrated. It is recommended that this interpretation capability be implemented in an on-line system with the real-time classifiers developed in this study in a prototype system using the remote communications capability deployed for this research project. Software for transforming proprietary data

formats from commercial AE instrumentation suppliers is available and pattern classifiers can be deployed in real-time versions. Such a system will provide reliable input with minimal interpretation requirements for inspection-based maintenance management.

2. The project has established that crack signals can be differentiated and separated from the substantial noise background using the artificial intelligence/pattern recognition methods described in the report. Hence, it is recommended to develop a fatigue cracking signal characteristic database using the typical steel and welds used in Michigan bridges. This database will help further refine the capability of the proposed automated system. Further, availability of signal characteristics to the AE monitoring system data analysts will help understanding the type of signals arise from the zones of interest.
3. Select representative bridges following the recommended process for Tier II implementation shown in Figure 6-1. Implement the AE monitoring system with the on-line signal classification system at a half dozen sites to gather data from typical fatigue-sensitive details to identify optimal settings and to optimize other deployment issues.

7 REFERENCES

AASHTO. (2008). AASHTO LRFD Bridge Construction Specifications, Second Edition with up to 2008 Interims, American Association of State Highway and Transportation Officials. Washington, D.C.

AASHTO LRFD. (2013). AASHTO LRFD Bridge Design Specifications, 6th Edition, the American Association of State Highway and Transportation Officials, Washington, DC 20001.

Abaqus (2012). Analysis User's manual, Volume 4, Section 25.1.4, Version 6.12, Three-Dimensional Solid Element Library. Dassault Systemes Simulia Corp.

ABS (2013). Guide for the Fatigue Assessment of Offshore Structures. American Bureau of Shipping, ABS Plaza, 16855 Northchase Drive, Houston, TX 77060

ABS (1992). Guide for fatigue strength assessment of tankers, Part 3 Steel Vessel Rules. American Bureau of Shipping (ABS), Houston, TX 77060, USA.

Adams, C. A. (2010). "Finite Element Study on Bridge Details Susceptible to Distortion-induced Fatigue." *Masters Thesis*, University of Kansas, Lawrence, KS 66045, USA.

Åkesson, B. (2010). *Fatigue life of riveted steel bridges*. Taylor & Francis Group, London, UK.

Akhlaghi, F. Z., Al-Emrani, M., Fryba, L., and Urushadze, S. (2009). "Fatigue testing and analysis of an orthotropic bridge welded detail using structural hot spot stress method," *Fatigue Design 2009*, Cetim - Technical Centre for Mechanical Industries, Senlis, France, November 25 – 26.

Alemdar, F., Nagati, D., Matamoros, A., Bennett, C., and Rolfe, S. (2014a). "Repairing distortion-induced fatigue cracks in steel bridge girders using angles-with-plate retrofit technique. I: Physical simulations." *J. Bridge Eng.*, 10.1061/(ASCE)ST.1943-541X.0000876

Alemdar, F., Overman, T., Matamoros, A., Bennett, C., and Rolfe, S. (2014b). "Repairing distortion-induced fatigue cracks in steel bridge girders using angles-with-plate retrofit technique. II: Computer simulations." *J. Struct. Eng.*, 10.1061/(ASCE)ST.1943-541X.0000874, 04014004.

Alemdar, F., Matamoros, A. B., Bennett, C. R., Barrett-Gonzalez, R., and Rolfe, S. T. (2011). "Improved Method for Bonding CFRP Overlays to Steel for Fatigue Repair" *42st Structures Congress Conference 2011*, ASCE, Las Vegas, NV, USA.

Applied Ultrasonics. (2014). <http://www.appliedultrasonics.com/> (Last accessed: October 5, 2014).

ASTM E 976 (2010). "Standard Guide for Determining the Reproducibility of Acoustic Emission Sensor Response." ASTM International, 100 Barr Harbor Drive, PO Box C700, West Conshohocken, PA 19428-2959.

Aygul, M. (2012). Fatigue Analysis of Welded Structures Using the Finite Element Method. Thesis, Department of Civil and Environmental Engineering, Division of Structural Engineering, Steel and Timber Structures, Chalmers University of Technology, Gothenburg, Sweden.

Aygul, M., Al-Emrani, M., and Urushadze, S., (2012). "Modeling and Fatigue Life Assessment of Orthotropic Bridge Deck Details Using FEM." *The International Journal of Fatigue*, Vol. 40, p. 129-142.

Barut, S. (2006). "Use of piezoelectric films for NDT applications." *The 9th European NDT Conference (ECNDT)*, Berlin, German, September 25 - 26.

Bassetti, A., Nussbaumer, A., and Hirt M. A. (2000). "Crack Repair and Fatigue Life Extension of Riveted Bridge Members Using Composite Materials." *Proceedings of Bridge Engineering Conference: The Egyptian Society of Engineers*, v 1, p 227-238.

Bell, E.S., Peddle, J.T., and Goudreau, A. (2012). "Bridge Condition Assessment using Digital Image Correlation and Structural Modeling." *The 6th International Conference on Bridge Maintenance, Safety and Management*, Stresa, Lake Maggiore, Italy, July 8-12, 2012.

Berglund, E. M., and Schultz, A. E. (2006). "Girder Differential Deflection and Distortion-Induced Fatigue in Skewed Steel bridges." *Journal of Bridge Engineering*. Vol. 11, pp. 169-177.

Bhargava, A. (2010). Fatigue Analysis of Steel Bridge Details: Hot Spot Stress Approach. Doctor of Philosophy Dissertation, the George Washington University, Washington, DC 20052.

Bhargava, A., and Roddis, W. M. K. (2007). *Finite Element Analysis of Fatigue Prone Details of the Tuttle Creek Bridge*. Report No. KS-07-5, Kansas Department of Transportation.

Bowman, M. D., Fu, G., Zhou, T. E., Connor, R. J., and Godbole, A. A. (2012). *Fatigue Evaluation of Steel Bridges*. NCHRP Report 721, Transportation Research Board of the National Academies, Washington, D.C.

Chakarav, K., Garbatov, Y., and Soares, C. G. (2008). "Fatigue analysis of ship deck structure accounting for imperfections," *International Journal of Fatigue*, Vol. 30, pp. 1881–1897.

Cintron, R., and Saouma, V. (2008). *Strain Measurements with the Digital Image Correlation System Vic-2D*. Center for Fast Hybrid Testing, Department of Civil and Environmental and Architectural Engineering, University of Colorado, UCB 428, Boulder, Colorado.

Det Norske Veritas (DNV) (2011). *Fatigue Design of Offshore Steel Structures*. Recommended Practice DNV-RP-C203, Det Norske Veritas.

Dexter, R. J., and Ocel, J. M. (2013). *Manual for Repair and Retrofit of Fatigue Cracks in Steel Bridges*. Technical Report FHWA-IF-13-020, Federal Highway Administration, McLean, VA 22101.

DFT UK (2006). *Design Manual for roads and bridges*. Report no. BA 86/06. Department for Transport, UK.

Ettah, E. B., Udoimuk, A. B., Obiefuna, J. N., and Opara, F. E. (2012). "The Effect of Relative Humidity on the Efficiency of Solar Panels in Calabar, Nigeria", *Universal Journal of Management and Social Sciences*, Vol. 2, No. 3, March 2012, pp. 8-11.

Eurocode 9, 1998. *Design of aluminum structures - Part 2: Structures susceptible to fatigue*. EN 1999-2:1998 E, British Standard, London.

Fasl, J. (2013). "Using NI WSN and LabVIEW to Wirelessly Monitor Fatigue Damage on Highway Bridges." The University of Texas at Austin.

<<http://sine.ni.com/cs/app/doc/p/id/cs-15206>> (Last accessed: March 29, 2013).

Fasl, J., Helwig, T., Wood, S.L., (2013) “Probabilistic method for estimating remaining fatigue life in steel bridges using measured strain data.” *Journal of Civil Structural Health Monitoring*. Vol. 3, Issue 4. pp. 317-324.

Fasl, J., Samaras, V., Reichenbach, M., Helwig, T., Wood, S.L., Potter, D., Lindenberg, R., and Frank, K. (2012). "Development of a Wireless Strain Node and the Software to Monitor Fracture-Critical Bridges." *Proc. SPIE 8347*, Nondestructive Characterization for Composite Materials, Aerospace Engineering, Civil Infrastructure, and Homeland Security 2012, 83471R (April 26, 2012).

FHWA (2012). *Feasibility of Nondestructive Crack Detection and Monitoring for Steel Bridges*. Report No. FHWA-HRT-12-060, Final Report, June 2006-March 2012, NDE Center, Federal Highway Administration, McLean, VA 22101.

Fisher, J.W., Statnikov, E., Tehini, L. (2001). “Fatigue Strength Enhancement by Means of Weld Design Change and the Application of Ultrasonic Impact treatment.” *Proceedings of the International Symposium on Steel Bridges*, Chicago.

Fisher, J. W., Jin, J., Wagner, D., and Yen, B. (1990). *Distortion Induced Fatigue Cracking in Steel Bridges*. NCHRP Report 336, Transportation Research Board, National Research Council. Washington D.C.

Fisher, J., Barthelemy, B., and Mertz, D. (1980). *Fatigue behavior of full-scale welded bridge attachments*. National Cooperative Highway Research Program (NCHRP) 227. Transportation Research Board. Washington, D.C.

Fisher, J. W. (1984). *Fatigue and fracture in steel bridges – Case studies*. John Wiley & Sons, New York.

Fricke, W. and Kahl, A. (2005). “Comparison of different structural stress approaches for fatigue assessment of welded ship structures,” *Marine Structures*, Vol. 18, pp. 473–488.

Fricke, W., Petershagen, H., and Paetzold, H. (1998). *Fatigue Strength of Ship Structures-Example*. GL-Tech.

http://www.gl-group.com/pdf/GL_Technology_Part_II_Examples.pdf (Last Accessed: 09/21/2014).

Fu, G., Feng, J., Dekelbab, W., Moses, F., Cohen, H., Mertz, D., and Thompson, P. (2003). *Effect of Truck Weight on Bridge Network Costs*. NCHRP Report 495, Transportation Research Board, Washington DC 20001.

Ghahremani, K., Sadhu, A., Walbridge, S., and Narasimhan, S. (2013). "Fatigue Testing and Structural Health Monitoring of Retrofitted Steel Highway Bridge Web Stiffeners." 92nd TRB Annual Meeting. Transportation Research Board, Washington DC 20001, January 13-17, 2013.

Gregory, E., Slater, G., and Woodley, C. (1989). *Welded repair of cracks in steel bridge members*. National Cooperative Highway Research Program (NCHRP) 321. Transportation Research Board. Washington, D.C.

Gunther, H. P., Kuhlmann, U., and Durr, A. (2005). "Rehabilitation of Welded Joints by Ultrasonic Impact Treatment (UIT)." *The International Association for Bridge and Structural Engineering (IABSE) Symposium*, Lisbon.

Hacini, L., Van Lê, N., and Bocher, P. (2008). "Effect of impact energy on residual stresses induced by hammer peening of 304L plates." *Journal of Materials Processing Technology*, v 208, n 1-3, p 542-548.

Hassel, H. L. (2011). "An Analytical Evaluation of Distortion-Induced Fatigue in Steel Bridges." Master's Thesis, University of Kansas.

Hassel, H. L., Hartman, A. S., Bennett, C. R., Matamoros, A. B., and Rolfe, S. T. (2010). "Distortion-Induced Fatigue in Steel Bridges: Causes, Parameters, and Fixes," Proceedings ASCE Structures Congress 2010, Orlando, Florida, May 12 – 15.

Hay, D.R. and Nyborg, E.O. (2000). *Acoustic emission handbook*, TISEC Inc. Morin Heights, Quebec, Canada J0R 1H0.

Hay, D.R., Cavaco, J.A., and Mustafa, V. (2009). "Monitoring the Civil Infrastructure with Acoustic Emission: Bridge Case Studies." *J. Acoustic Emission*, Vol. 27, pp. 1- 10.

Hee T. Y. and Isa, M. M. (2009). "Design of a mini solar power system," Proceeding of 2009 IEEE Student Conference on Research and Development, UPM Serdang, Malaysia, Nov. 16 – 18.

Huang, M., Jiang, L., Liaw, P.K., Brooks, C.R., Seeley, R., and Klarstrom, D.L. (1998). "Using Acoustic Emission in Fatigue and Fracture Materials Research." *JOM*, vol. 50, no. 11, November 1998.

Hobbacher, A. (2008). Recommendations for Fatigue Design of Welded Joints and Components. International Institute of Welding (IIW), doc. XIII-2151r4-07/XV-1254r4-07. Paris, France.

Hu, Y., Shield, C. K., and Dexter, R. J. (2006). *Use of Adhesives to Retrofit Out-of-Plane Distortion Induced Fatigue Cracks*. MN/RC-2003-04, Report to the Minnesota Department of Transportation, St. Paul, MN 55155

Iadicola, M.A., Zobel, R.S., and Ocel, J.M. (2012). "Quantitative evaluation of digital image correlation as applied to large-scale gusset plate experiments." The 6th International Conference on Bridge Maintenance, Safety and Management, Stresa, Lake Maggiore, Italy, July 8-12, 2012.

ICEPak® (2014). <http://structuralinsights.com/AI/specification.php> (Last accessed: Dec. 02, 2014)

Ju, X., and Tateishi, K. (2012). "Structure on Fatigue Crack Propagation of a Through-thickness Crack Subjected to Out-of-plane bending." *International Journal of Steel Structures*, Vol. 12, No. 1, pp. 85-92.

Kaphle, M., Tan, A. C. C., Thambiratnam, D. P., and Chan, T. H. T. (2012). "A Study on the Use of Acoustic Emission Technique as a Structural Health Monitoring Tool." *Journal of Engineering Asset Management and Infrastructure Sustainability*, pp. 459 - 469.

Kaur, M., Sandhu, M., Mohan, N., and Sandhu, P. S. (2011). "RFID Technology Principles, Advantages, Limitations & Its Applications." *International Journal of Computer and Electrical Engineering*, Vol. 3, No. 1, pp. 151 – 157.

Kazem, H. A., Chaichan, M. T., Al-Shezawi, I. M., Al-Saidi, H.S., Al-Rubkhi, H. S., Al-Sinani, J. K. and Al-Waeli, A. H. A. (2012). "Effect of Humidity on the PV Performance in Oman," *Asian Transactions on Engineering* (ATE ISSN: 2221 - 4267), Vol. 02, Issue 04, pp. 29 – 32.

Kosnik, D.E. (2008). "A New Approach to Acoustic Emission Testing of Difficult-to-Reach Steel Bridge Details." Infrastructure Technology Institute / Department of Civil & Environmental Engineering, Northwestern University, Evanston, Illinois 60208, USA.

Kühn, B., Lukić, M., Nussbaumer, A., Günther, H. P., Helmerich, R., Herion, S., Kolstein, M. H., Walbridge, S., Androic, B., Dijkstra, O., and Bucak, Ö. (2008). "Assessment of Existing Steel Structures: Recommendations for Estimation of Remaining Fatigue Life," EUR 23252 EN – 2008, European Commission, Joint Research Centre, Brussels – Belgium.

Kujawski, D., Ghantasala, M.; Gokanakonda, S.; and Hussain, S. (2011). Structural health diagnosis and prognostics using fatigue monitoring. SAE 2011 World Congress and Exhibition, Detroit, MI.

Ledeczi, A., Hay, T., Vogyesi, P., Hay, D.R., Nadas, A. and Jayaraman, S. (2009). "Wireless Acoustic Emission Sensor Network for Structural Monitoring." *IEEE Sensors Journal*, Vol. 9, No. 11, November 2009.

Lee, J. M., Seo, J.K., Kim, M.H., Shin, S.B., Han, M.S., Park, J.S., and Mahendran, M. (2010). "Comparison of Hot Spot Stress Evaluation Methods for Welded Structures." *The International Journal of Naval Architecture and Ocean Engineering*, Vol. 4 (2), pp. 200-210.

Leander, J., Andersson, A., Karoumi, R. (2010). "Monitoring and enhanced fatigue evaluation of a steel railway bridge." *Engineering Structures*. Vol. 32, pp. 854-863.

Leon, A. (1998). "Benefits of Split Mandrel Coldworking." *International Journal of Fatigue*, v 20, n 1, p 1-8.

Li, Z.X., Chan, T.H.T., Ko, J.M. (2001). "Fatigue damage model for bridge under traffic loading: application made to Tsing Ma Bridge." *Theoretical and Applied Fracture Mechanics*, Vol. 35, pp. 81-91.

Li, H., and Schultz, A. E. (2005). *Analysis of Girder Differential Deflection and Web Gap Stress for Rapid Assessment of Distortional Fatigue in Multi-Girder Steel Bridges*. MN/RC-2008-38, Report to the Minnesota Department of Transportation, St. Paul, MN 55155.

Li, F., Xiang, D., Chiang, S., Tittmann, B. R., and Searfass, C. (2011). "Wireless surface acoustic wave radio frequency identification (SAW-RFID) sensor system for temperature and strain measurements." IEEE International Ultrasonics Symposium 2011 (IUS 2011), October 18-21, 2011, Caribe Royale, Orlando, Florida, USA.

Lovejoy, S.C. (2003). "Determining Appropriate Fatigue Inspection Intervals for Steel Bridge Members." *Journal of Bridge Engineering*. Vol. 8, No .2, pp. 66-72.

McCrea, A., Chamberlain, D., and Navon, R. (2002). "Automated inspection and restoration of steel bridges—a critical review of methods and enabling technologies." *Journal of Automation in Construction*, Vol. 11, pp. 351 – 373

MBE. (2011). *The Manual of Bridge Evaluation*, 2nd Edition, the American Association of State Highway and Transportation Officials, Washington, DC 20001.

MDOT (2009). "Michigan Bridge Analysis Guide," the Michigan Department of Transportation, Lansing, Michigan, 48909.

http://www.michigan.gov/documents/mdot/MDOT_2009__InterimBridgeAnalysisGuide_Part1_274530_7.pdf . (Last accessed: September 2014)

Mentes, Y. (2011). Analytical and experimental analysis of steel truss bridge gusset plate connections. A Dissertation Presented to The Academic Faculty, Georgia Institute of Technology, December 2011.

Metal Fatigue Solutions, Inc. (MFS) (2014). <http://www.metal-fatigue-solutions.com/technology/> (Last accessed: October 26, 2014).

Moshier, M. and Berks, W. I. (2009). Electrochemical fatigue sensor systems and methods United States Patent, US 7,572,360 B2.

Moshier, M. A., Miceli, M., Le, H., and Leach, D. (2009). "Inspection of Fatigue Cracks on a CN Bridge Using the Electrochemical Fatigue Sensor." The AREMA 2009 Annual Conference & Exposition, September 20 – 23, 2009, Chicago, IL.

NASA. (2014). NASA Langley Research Center Atmospheric Science Data Center, https://eosweb.larc.nasa.gov/project/sse/sse_table. Accessed July 12, 2014

Nair, A., and Cai, C.S. (2010). "Acoustic emission monitoring of bridges: Review and case studies." *Engineering Structures*, Vol. 32, No. 6, pp. 1704-1714.

NDT (2014). NDT Resource Center, the Collaboration for NDT Education, Iowa State University. <www.ndt-ed.org> (Last accessed: December 17, 2014).

NREL. (2014). The National Renewable Energy Laboratory. <http://www.nrel.gov/gis/solar.html> (Last accessed: November 27, 2014).

Nguyen, K. T., Garbatov, Y., and Soares, C. G. (2012). "Fatigue damage assessment of corroded oil tanker details based on global and local stress approaches," *International Journal of Fatigue*, Vol. 43, pp. 197–206.

Niemi E (1993). "Stress determination for fatigue analysis of welded components. IIW Doc. IIS/IIW-1221-93", International Institute of Welding.

Niemi, E., Fricke, W., and Maddox, S.J. (2006). "Fatigue Analysis of Welded Components: Designer's guide to the structural hot-spot stress approach (IIW-1430-00)", Cambridge: Woodhead Publishing Limited.

Ozelton, M. W., and Coyle, T. G. (1986). "Fatigue Life Improvement by Cold Working Fastener Holes in 7050 Aluminum." *Fatigue in Mechanically Fastened Composite and Metallic Joints, ASTM STP 927*. Ed. John M. Potter. Philadelphia: ASTM, p 53-71.

Parmar, D.S. and Sharp, S.R. (2009). "Acoustic Emission for Non-Destructive Testing of Bridges and Other Transportation Infrastructure." Beyond the Crossroads: A National Conference on Transportation Infrastructure & Regulatory Policy. May 27-28, 2009. University of Denver, Denver, CO.

Phares, B.M. (2007). "The electrochemical fatigue sensor: A novel sensor for active fatigue crack detection and characterization." The 3rd Conference on Structural Health Monitoring of Intelligent Infrastructure, Vancouver, British Columbia, Canada, November 13-16, 2007.

Pook, L. (2007). *Metal Fatigue, what it is, why it matters*. Springer, P.O.Box 17, 3300 AA Dordrecht, the Netherlands.

Proto Manufacturing Inc., Universal Drive, Taylor, Michigan, USA. <protoxrd.com> (Last accessed: March 29, 2013).

Ramchandra, P., Boucar, D. (2011). *Solar Lighting*. Springer-Verlag, New York.

Reijmers, J., (2002). The Extrapolation of Finite Element Result to Hot Spot Stresses. Presentation. IV Nevesbu, Papendrecht, Netherlands.

file:///C:/Users/attupul/Downloads/FENET_Glasgow_Oct2004_EDU_Reijmers.pdf (Last Accessed: 09/21/2014).

Rose, J.L., and Royer, R.L. (2008). "A Guide wave Health Monitoring Approach for Civil Structures." 26th IMAC: Conference and Exposition on Structural Dynamics 2008 (IMAC XXVI), February 4-7, 2008, Orlando, Florida. Society for Experimental Mechanics (SEM).

Roy, S., Fisher, J., and Yen, B. (2003). "Fatigue Resistance of welded details enhanced by ultrasonic impact treatment (UIT)." *International Journal of Fatigue*. Vol. 25. pp. 1239-1247.

Schultz, A. and Thompson, D. (2010). *Development of an Advanced Structural Monitoring System*. Minnesota Department of Transportation, Research Services Section, St. Paul, MN 55155.

Shield, C. and McKeefry, J. (1999). *Acoustic Emission Monitoring of Fatigue Cracks in Steel Bridge Girders*. MN/RC – 1999-36, Minnesota Department of Transportation, St. Paul, MN 55155.

Shifferaw, Y., and Fanous, F. S. (2013). "Field Testing and Finite Element Analysis of Steel Bridge Retrofits of Distortion-Induced Fatigue." *Engineering Structures*, Vol. 49, 2013, pp. 385-395.

Shirahata, H., Ueda, N., Kishida, A. (2014). Development of monitoring system for bridge collapse detection by energy harvest with solar cell. *Bridge Maintenance, Safety, Management and Life Extension*, Taylor & Francis Group, London, pp. 1405-1410.

Stefanescu, D., Santisteban, J. R., Edwards, L., and Fitzpatrick, M. E. (2004). "Residual Stress Measurement and Fatigue Crack Growth Prediction after Cold Expansion of Cracked Fastener Holes." *Journal of Aerospace Engineering*, v 17, n 3, p 91-97.

Sunsaver. (2014). *Sunsaver MPPT Installation and Operation manual*. Morningstar Corp., Washington Crossing, PA. (Last accessed: July 12, 2014).

Tarries, D. J., Phares, B. M., Wipf, T. J., Greimann, L., Wood, D. L. (2002). "Bolt Loosening Retrofit to Inhibit Fatigue Cracking in Steel Girder Bridges." *82nd Annual Meeting, Transportation Research Board*, Washington, D. C.

Tianze, L., Hengwei, L., Chuan, J., Luan, H., Xia, Z. (2011). Application and design of solar photovoltaic system. *3rd International Photonics & OptoElectronics Meetings, Journal of Physics: Conference Series 276*.

Vallen (2013). <http://www.vallen.de/sites/default/files/sov1212.pdf> (Last accessed: 10/25/2013).

Wang, C., Tian, L., Fu, B., and Zhang, Y. (2012). "Fatigue cracking monitoring and evaluation using smart sensors for steel bridge decks." *The 6th International Conference on Bridge Maintenance, Safety and Management (IABMAS)*, Stresa, Lake Maggiore, Italy, July 8-12, 2012.

Wipf, T. J., Greimann, D. L., Wood, B. M., Tarries, D. (2003). *Retrofit methods for distortion cracking problems in plate girder bridges*. TR-436, Report to Iowa Highway Research Board, Ames, IA; 2003.

Yang, C. and Fritzen, C. P. (2011). "A novel piezoelectric paint sensor for nondestructive testing." *The International Workshop – Smart Materials, Structures & NDT in Aerospace*, Montreal, Quebec, Canada, November 2 - 4.

Yang, L., Smith, L., Gothekar, A., and Chen, X. (2010). *Measurement of Strain Distribution Using Digital Image Correlation (DIC) for Tensile Tests*. Final Report. The Advanced High Strength Steel Stamping Team of the Auto/Steel Partnership (A/SP). Southfield, Michigan.

Yekta, T. R., Ghahremani, K., and Walbridge, S. (2013). "Effect of quality control parameter variations on the fatigue performance of ultrasonic impact treated welds." *International Journal of Fatigue*, 55:245-256.

Yi, X., Ruchi, V., Chunhee, C., Chia-Hung, F., Cooper, J., Wang, Y., Leon, R.T., and Tentzeris, M.M. (2012a). "Thermal effects on a passive wireless antenna sensor for strain and crack sensing." Proceedings of SPIE - The International Society for Optical Engineering, San Diego, CA, United states, March 12 - 15, 2012.

Yi, X., Wang, Y., Leon, R.T., Cooper, J., and Tentzeris, M.M. (2012). "Wireless crack sensing using an RFID-based folded patch antenna." The 6th International Conference on Bridge Maintenance, Safety and Management (IABMAS), Stresa, Lake Maggiore, Italy, July 8-12, 2012.

Yildirim, H. C. and Marquis, G. B. (2011). *Fatigue of welded components and structures: Overview of fatigue data for high frequency treated welded joints*. A report to the COMMISSION XIII, International Welding Institute (IIW).

Yoneyama, S., Kitagawa, A., Iwata, S., Tani, K., and Kikuta, H. (2007). "Bridge Deflection Measurement using Digital Image Correlation." *Experimental Techniques*, Volume 31, Issue 1, January/February 2007, pp. 34-40.

Yu, J., Ziehl, P., Zarate, B., and Caicedo, J. (2011). "Prediction of fatigue crack growth in steel bridge components using acoustic emission." *Journal of Constructional Steel Research*, Vol. 67, pp. 1254 - 1260.

Zhang, Y., Zhou, C., Fu, C.C., and Zhou, Y.E. (2013). "Field Monitoring of Fatigue Crack on Highway Steel I-girder Bridge." 92nd TRB Annual Meeting. Transportation Research Board, Washington DC 20001, January 13-17, 2013.

Zhao, X., Gao, H., Zhang, G., Ayhan, B., Yan, F., Kwan, C., and Rose, J.L. (2007). "Active Health Monitoring of and Aircraft Wing with Embedded Piezoelectric Sensor/actuator network: I. Defect Detection, Localization, and Growth Monitoring." *Smart Materials and Structures*, IOP Publishing, pp 1208-1217.

Zhao, X., Qian, T., Qi, K., Mei, G., Liu, A., Xu, R., and Zane, R. (2013). "A Novel Wireless Multi-sensor Network System for Steel Bridge Fatigue Crack Monitoring." 92nd TRB Annual Meeting. Transportation Research Board, Washington DC 20001, January 13-17, 2013.

Zhou, Y. E. (2005). "Assessment of Bridge Remaining Fatigue Life through Field Strain Measurement," ASCE Structures Congress 2005, New York, April 20-24.

Zhu, X, Rizzo, P., Marzani, A., and Bruck, J. (2010). "Ultrasonic guided waves for nondestructive evaluation/structural health monitoring of trusses." *Measurement Science and Technology*, Vol. 21, No. 4, pp. 1-12.